ACS OMEGA

Open Access

http://pubs.acs.org/journal/acsodf

Article

Synthesis and Evaluation of Thiazolyl-indole-2-carboxamide Derivatives as Potent Multitarget Anticancer Agents

Njood M. Saadan, Wahid U. Ahmed, Adnan A. Kadi, Maha S. Al-Mutairi, Reem I. Al-Wabli,* and A. F. M. Motiur Rahman*

Cite This: *ACS Omega* 2024, 9, 41944−41967

Read Online

ACCESS | Metrics & More | Article Recommendations | Supporting Information

ABSTRACT: Cancer is a complex disease driven by the dysregulation of multiple signaling pathways and cellular processes. The development of compounds capable of exerting multitarget actions against these key pathways involved in cancer progression is a promising therapeutic approach. Here, a series of novel (*E*/*Z*)-*N*-(4-(2-(2-(substituted)hydrazineyl)-2-oxoethyl)thiazol-2-yl)-1*H*-indole-2-carboxamide derivatives (**6a**−**6z**) were designed, synthesized, and evaluated for their biological activity. Compounds **6e**, **6i**, **6q**, **6v**, **7a**, and **7b** exhibited exceptional cytotoxicity against various cancer cell lines, particularly **6i** (IC_{50} = 6.10 ± 0.4 μM against MCF-7 cell lines) and **6v** (IC_{50} = 6.49 ± 0.3 μM against MCF-7 cell lines). These potent compounds inhibited key protein kinases like EGFR, HER2, VEGFR-2, and CDK2, induced cell cycle arrest at the G2/M phase, and promoted apoptosis. Docking studies revealed improved binding affinity of **6i** and **6v** with target proteins compared to reference drugs. These findings highlight the promising potential of **6i** and **6v** as multitarget cancer therapeutics deserving further development.

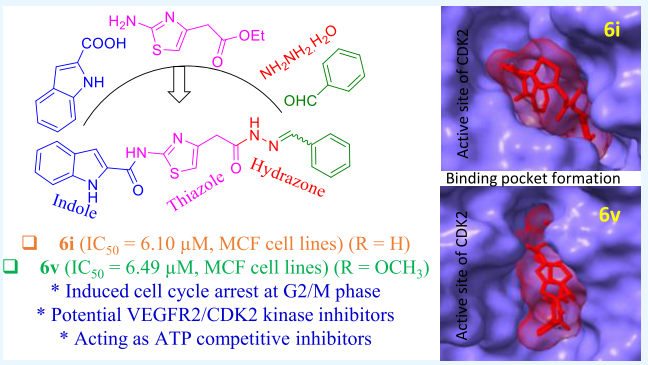

INTRODUCTION

Cancer is a global health concern, with significant incidence and mortality rates worldwide.[1] In Saudi Arabia, it is the second leading cause of death, prompting initiatives to improve research and interventions.[2,3] Cancer is a complex disease influenced by genetic, environmental, and lifestyle factors, resulting in abnormal cell growth.[4−7] Comprehensive understanding of these factors is crucial for implementing preventive measures and developing targeted interventions. Cancers are categorized based on the resemblance of tumor cells to specific cell types, indicating their presumed origin. The main categories include carcinomas, sarcomas, lymphomas and leukemias, germ cell tumors, and blastomas.[8−11] Early detection and personalized treatment plans are vital for improving outcomes in cancer patients. Polypharmacology,[12] a subfield focusing on multitarget compounds,[13] offers promising solutions to overcome drug resistance and improve treatment efficacy. Cancer development involves complex cellular and molecular mechanisms,[14] including genetic mutations,[15] activation of oncogenes,[16] inactivation of tumor suppressor genes,[17] genomic instability,[18] and dysregulation of signaling pathways.[18−21] Understanding these mechanisms guides the development of targeted therapies and immune-based approaches to combat cancer. Cancer diagnosis involves a range of imaging techniques,[22] such as X-ray, ultrasound,[23] CT scans,[24] and MRI,[24] fluorescence imaging technique,[25,26] boron neutron therapy (BNCT),[27−30] positron emission tomography (PET),[31,32] to visualize tumors and assess their characteristics. Laboratory tests, including blood tests[33] and biopsies,[34] are also used to detect cancer and examine tissue samples for cancer cells. Staging systems,[35] such as the TNM system,[36] help determine the extent of tumor growth, lymph node involvement, and distant metastasis, providing a standardized approach to guide treatment decisions and predict prognosis. Accurate diagnosis and staging are crucial for effective cancer management and monitoring treatment outcomes.[37] Cancer management involves a variety of treatment modalities tailored to individual patient needs. Surgical intervention aims to remove tumors,[38] while radiation therapy uses high-energy radiation to destroy cancer cells.[37] Chemotherapy[39] targets rapidly dividing cells, immunotherapy[40] enhances the immune response against cancer, and targeted therapies[41] address specific molecular abnormalities. Hormone therapy[42] disrupts hormone-driven growth, and combination therapies aim for improved outcomes. Personal-

Received: July 26, 2024
Revised: September 16, 2024
Accepted: September 19, 2024
Published: September 24, 2024

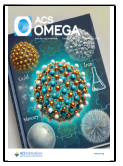

Chart 1. Some Examples of Indole/Thiazole-Containing Marketed Anticancer Drugs

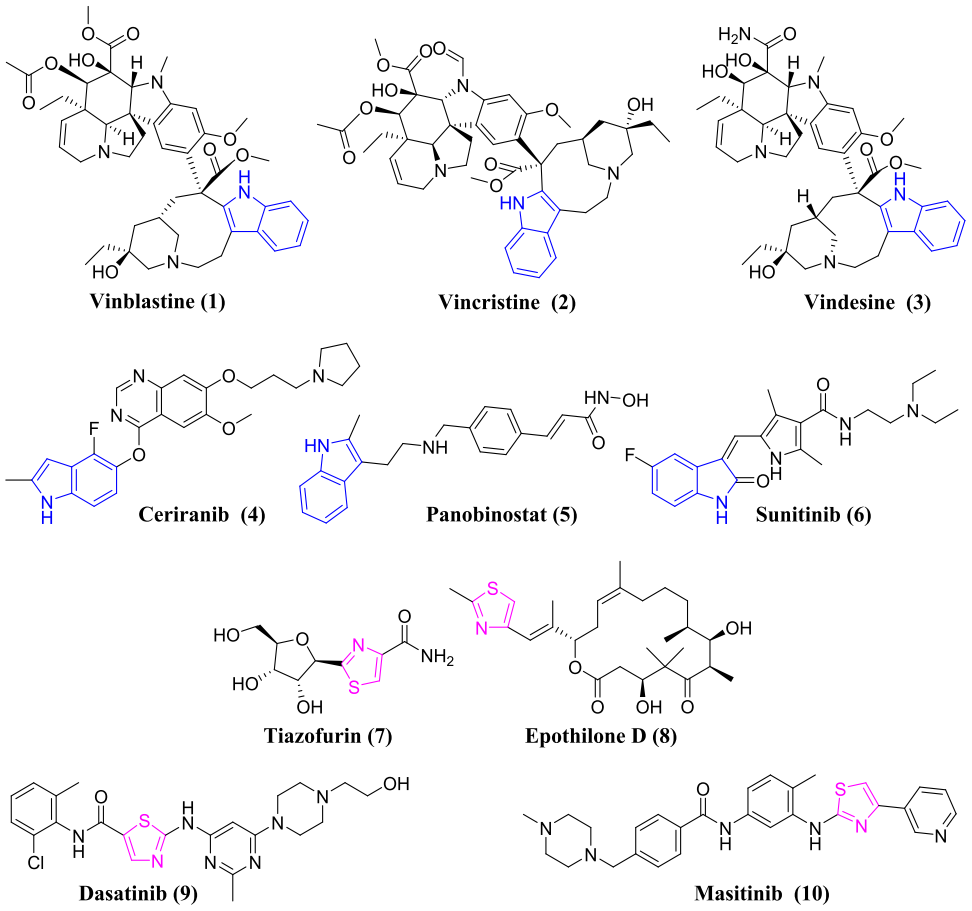

Chart 2. Example of Some Hydrazine-Containing Known Drugs and Recently Reported Molecules

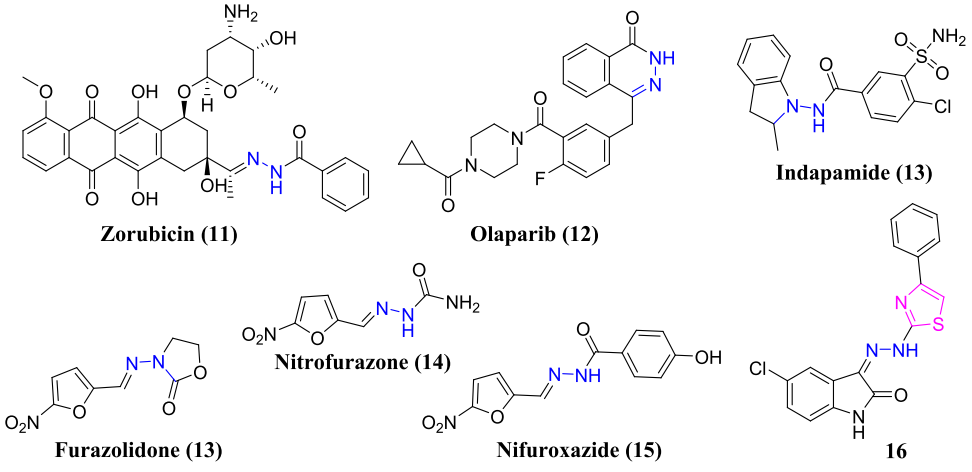

ized treatment plans consider cancer characteristics, stage, patient health, and preferences to optimize effectiveness and minimize side effects. Innovations like precision medicine and personalized therapy[43] base treatments on genetic profiles and tumor characteristics.[44] Immunotherapies, including immune checkpoint inhibitors[45] and CAR-T cell therapy,[46] have transformed cancer treatment by boosting the immune response. Key areas of research focus on overcoming drug resistance and targeting tumor heterogeneity and the tumor microenvironment. Tyrosine kinases, which play a critical role in cell signaling and are often overexpressed in cancers, are rational targets for therapy.[47−49] Inhibiting tyrosine kinases, such as EGFR, HER2, and VEGFR-2, disrupts tumor growth signaling, and tyrosine kinase inhibitors (TKIs) have emerged as effective targeted therapies.[50−55] Ongoing research seeks to identify new therapeutic targets and optimize strategies for various cancers, underscoring the continuous pursuit of improved treatments.

Heterocyclic compounds, such as indoles and thiazoles, have revolutionized cancer therapy (Chart 1).[56−59] The success of the tyrosine kinase inhibitor (TKI) imatinib in treating chronic myeloid leukemia inspired the exploration of heterocyclic-

https://doi.org/10.1021/acsomega.4c06889
ACS Omega 2024, 9, 41944−41967

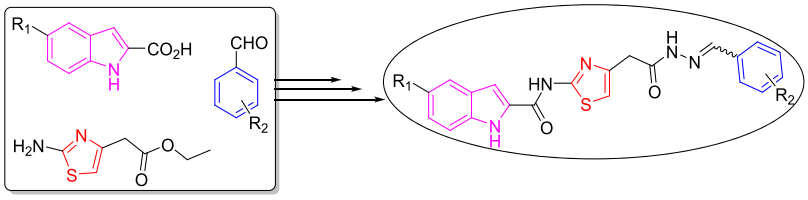

Figure 1. Designed potential TKI from indole, triazole, and aldehydes.

based TKIs for various cancers.[60] These compounds selectively target proteins involved in cancer signaling pathways, like EGFR, HER2, and VEGFR, leading to improved efficacy and reduced side effects.[61] Indole-based compounds have demonstrated versatility in targeting multiple molecular pathways critical for cancer progression, including inhibition of protein kinases, tubulin assembly, and DNA repair enzymes.[62] Indoles can also induce apoptosis and modulate gene expression, contributing to their potential as anticancer agents.[62,63] Thiazole derivatives, such as tiazofurin and epothilone D, exhibit diverse mechanisms of action in cancer treatment, including inhibition of nucleotide metabolism, microtubule stabilization, and targeting of tyrosine kinases.[64−66] Dasatinib and masitinib, two notable thiazole-based TKIs, have shown therapeutic potential in treating chronic myeloid leukemia, acute lymphoblastic leukemia, and other cancers.[67−71] The versatility and broad range of biological activities associated with heterocyclic compounds, particularly indoles and thiazoles, continue to drive research and innovation in the field of anticancer drug discovery. Ongoing exploration of these scaffolds holds great promise for the development of novel, more effective, and targeted cancer therapies.[56−59]

Hydrazide/hydrazone-containing compounds have demonstrated remarkable versatility and significant contributions in various medical fields (Chart 2). Examples include Zorubicin,[72−74] an anthracycline anticancer drug; Nifuroxazide, an antibiotic; Olaparib, a PARP inhibitor for cancer treatment;[75,76] Indapamide, a diuretic for hypertension management; Furazolidone and Nitrofurazone, antibiotics for infections; and Bisantrene, an anticancer agent.[77−80] These compounds exhibit diverse mechanisms of action, ranging from inhibiting DNA replication to modulating ion transport and protein synthesis. The successful utilization of hydrazide/hydrazone compounds highlights their potential for further exploration and development in drug discovery. Fragment hybridization, combining multiple bioactive fragments into a single molecule, offers a promising strategy in medicinal chemistry for creating novel compounds with improved therapeutic efficacy.[81]

Masitinib, a potent compound with significant applications in cancer treatment, is synthesized through a complex multistep process involving the protection, deprotection, and coupling of various intermediate compounds, ultimately resulting in the formation of the desired product.[71,82−86] Sunitinib, a potent anticancer drug used for the treatment of certain malignancies, is synthesized through a multistep pathway involving reactions such as nitration, hydroxyimine formation, esterification, condensation, hydrolysis, and coupling, which result in the construction and modification of key functional groups leading to the final product.[87−94] Dasatinib, a potent anticancer drug, can be synthesized through various methods involving condensation reactions and subsequent modifications of key intermediates.[67−70,95−100] However, some of the synthesis routes involve multiple steps and require the use of hazardous reagents, which can be time-consuming, costly, and pose challenges in terms of process scalability. Therefore, the synthesis of dasatinib may have disadvantages such as complexity, potential safety concerns, and limitations in large-scale production.

As we have learned from the above discussion, the indole and thiazole heterocycles are privileged structures in medicinal chemistry, known for diverse biological activities. Indole-based compounds are potent and selective kinase inhibitors, targeting cancer signaling, while thiazole-containing compounds exhibit a range of pharmacological effects. Connecting indole and thiazole through an amide bond and hydrazide creates a unique scaffold with enhanced properties - the amide facilitates hydrogen bonding to improve affinity and selectivity, and the hydrazide can undergo redox/chelation for alternative mechanisms. This combination of privileged heterocycles may yield synergistic effects, enabling targeting of multiple pathways in cancer, providing a versatile platform for potent and selective anticancer agents. Therefore, in this report, we aim to develop novel and more effective anticancer therapeutics by combining an indole nucleus with a thiazole ring, creating a class of *N*-thiazolyl-indole-2-carboxamide compounds similar to dasatinib (Figure 1). These hybrid molecules are modified through hydrazone formation, resulting in a series of novel derivative. Using a concise three-step synthetic strategy, we aim to overcome limitations of current cancer therapies and provide accessible and promising treatment options with enhanced potency and selectivity.

RESULTS AND DISCUSSION

Synthesis of (*E*/*Z*)-*N*-(4-(2-(2-(Substituted)-hydrazineyl)-2-oxoethyl)thiazol-2-yl)-1*H*-indole-2-carboxamide (6a−6z). 1*H*-indole-2-carboxylic acid (**1a**) were reacted with ethyl-2-(2-aminothiazol-4-yl)acetate (**2**) to prepare ethyl-2-(2-(1*H*-indole-2-carboxamido)thiazol-4-yl)-acetate (**3a**) through peptide coupling reaction procedure. Initially, the reaction was carried out using *N*,*N*′-dicyclohexylcarbodiimide (DCC), thinking of the presence of bulky moieties (indole, **1a** and thiazole, **2**) as well as considering the inexpensive DCC along with 4-dimethylaminopyridine (DMAP) as coupling agents in CH_2Cl_2 at temperatures ranging from 0 °C to room temperature but failed to get 100% conversion. In addition to less conversion rate, a great difficulty was faced to purify the product because of unreacted starting materials and by product dicyclohexylurea (DCU). Later on, uses of 1-Ethyl-3-(3-(dimethylamino)propyl)carbodiimide (EDC) instead of DCC with same reaction condition, the reaction proceeded good to moderate yields (76%) (Table S1). The structure of **3a** were elucidated using 1D and 2D NMR analysis (Please see supporting file). In the second steps, compound **3a** was treated with hydrazine monohydrate to obtain *N*-(4-(2-hydrazineyl-2-oxoethyl)thiazol-2-yl)-1*H*-in-

https://doi.org/10.1021/acsomega.4c06889
ACS Omega 2024, 9, 41944−41967

Scheme 1. Synthesis of (*E*/*Z*)-*N*-(4-(2-(2-(Substituted)hydrazineyl)-2-oxoethyl)thiazol-2-yl)-1*H*-indole-2-carboxamide (6a−6z)

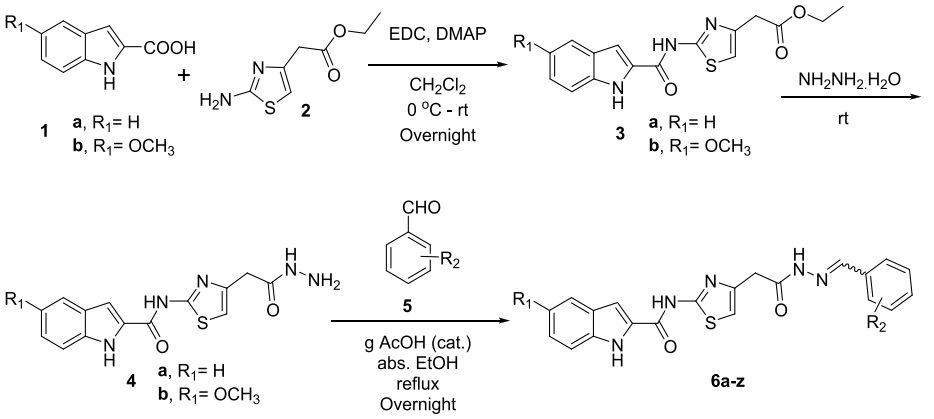

Number	R_1	R_2	Number	R_1	R_2
6a	H	H	**6n**	OCH_3	4-Br
6b	H	4-Br	**6o**	OCH_3	4-Cl
6c	H	4-Cl	**6p**	OCH_3	4-F
6d	H	4-F	**6q**	OCH_3	4-OH
6e	H	4-OH	**6r**	OCH_3	4-CH_3
6f	H	2-OCH_3	**6s**	OCH_3	2-OCH_3
6g	H	4-OCH_3	**6t**	OCH_3	4-OCH_3
6h	H	4-NO_2	**6u**	OCH_3	4-NO_2
6i	H	4-$N(CH_3)_2$	**6v**	OCH_3	4-$N(CH_3)_2$
6j	H	4-SCH_3	**6w**	OCH_3	4-SCH_3
6k	H	2-OH & 4-OCH_3	**6x**	OCH_3	3,4-di-Cl
6l	H	Naphthyl	**6y**	OCH_3	2-OH & 4-OCH_3
6m	OCH_3	H	**6z**	OCH_3	Naphthyl

dole-2-carboxamide (**4a**). In this step, the great problem was overcome. According to the literature procedure for hydrazide formation, ester was refluxed using hydrazine hydrate in the presence of EtOH (Method A) but interestingly a byproduct, namely, 1*H*-indole-2-carbohydrazide (**3c**) was obtained in large quantity without having **4a**. While at room temperature in EtOH (Method B) as well as without solvent at 100 °C (Method C) gave a mixture of starting material (**3a**), byproduct (**3c**) and a trace amount of desire product **4a**. Finally, at room temperature with neat condition (Method D) obtained **4a** with 100% conversion rate. The transformation provided excellent yields, reaching approximately 98% (Table S2).

To expand the molecular diversity, compounds (**4a**/**4b**) were subjected to condensation reactions with one equivalent of substituted aldehydes (**5**). The reactions were carried out in absolute ethanol, in the presence of a catalytic amount of glacial acetic acid. The desired products, namely (*E*/*Z*)-*N*-(4-(2-(2-(substituted)hydrazineyl)-2-oxoethyl)thiazol-2-yl)-1*H*-indole-2-carboxamide (**6a−6z**), were obtained in quantitative yields, ranging from approximately 96% to 100% (Scheme 1).

Overall, this synthetic approach showcases the potential of the developed methodology for the efficient synthesis of diverse compounds. It was surprising that all the final product was obtained as *E*/*Z* isomers, around 1 to 0.7−0.8 ratios. Proton and carbon NMR of all the compounds was carefully analyzed and elucidated the structures of compounds **6a−6z**. In brief, three -NH peaks were obtained with six different chemical shifts at around 11.71 to 11.15 ppm. *N*-Benzylidine protons were obtained with the difference of around 0.2 ppm in between 7.9 to 8.5 ppm. Protons at $-CH_2$ carbon was shown with 2.3 ppm difference at around 35 to 38 ppm. Thiazole ring singlet were shown with two singlets at around 6.9 to 7.1 ppm with 0.03−0.05 ppm difference. In addition, carbon containing $-CH_2$ was obtained around 35−40 ppm with the differences of 2.2−2.5 ppm. For an example, compounds **6a**s' *N*-benzylidine protons proton were shown at 8.22 and 8.00 ppm, protons at $-CH_2$ carbon was shown at 4.09 and 3.65 ppm, proton at thiazole ring were shown at 7.03 and 7.01 ppm, three -NH peaks were shown at 11.69 (2 peaks overlapped), 11.87, 11.86, 11.57, and 11.45 ppm, and carbon containing $-CH_2$ was appeared at 38.91 and 35.52 ppm, respectively (Figure 2).

Synthesis of 2-(2-(1*H*-Indole-2-carboxamido)thiazol-4-yl)acetic Acid (7a and 7b) and *N*-(4-(2-(Hydroxyamino)-2-oxoethyl)thiazol-2-yl)-1*H*-indole-2-carboxamide

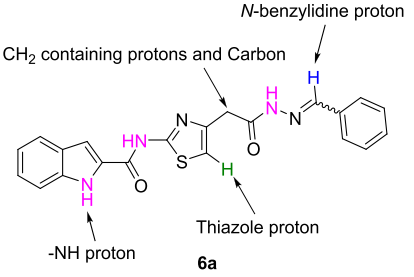

Figure 2. Structure of compound **6a**: showing the protons and carbons that give chemical shifts at different ppm values for the *E* and *Z* isomers.

https://doi.org/10.1021/acsomega.4c06889
ACS Omega 2024, 9, 41944−41967

Scheme 2. Synthesis of 2-(2-(1*H*-Indole-2-carboxamido)thiazol-4-yl)acetic Acid (7a/b) and *N*-(4-(2-(Hydroxyamino)-2-oxoethyl)thiazol-2-yl)-1*H*-indole-2-carboxamide (8a/b)

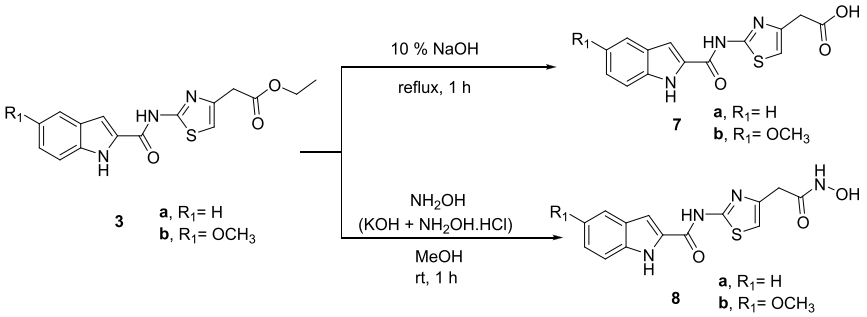

Table 1. *In Vitro* Cytotoxicity of Compounds 6a−6z, 7a, 7b, 8a, and 8b against Selected Cancer Cell Lines

	in vitro cytotoxicity IC_{50} (μM)				
compound	HCT-116	HepG2	HeLa	MCF-7	WI-38
6a	65.37 ± 3.7	44.57 ± 2.5	37.25 ± 2.3	52.37 ± 2.9	18.21 ± 1.6
6b	78.91 ± 4.0	81.65 ± 4.5	68.27 ± 3.7	64.19 ± 3.5	18.76 ± 1.4
6c	81.18 ± 4.2	86.81 ± 4.6	72.34 ± 3.9	75.19 ± 3.9	47.61 ± 2.8
6d	70.62 ± 3.8	74.78 ± 4.1	62.34 ± 3.4	59.22 ± 3.2	33.81 ± 2.3
6e	23.86 ± 1.7	69.63 ± 3.7	16.18 ± 1.2	9.28 ± 0.7	71.90 ± 3.9
6f	89.12 ± 4.6	94.30 ± 5.1	77.10 ± 4.1	82.13 ± 4.2	46.32 ± 2.6
6g	83.08 ± 4.1	>100	85.33 ± 4.4	79.28 ± 4.1	>100
6h	42.30 ± 2.5	26.59 ± 1.9	24.57 ± 1.8	30.07 ± 2.0	76.93 ± 4.1
6i	9.69 ± 0.8	32.74 ± 2.1	4.36 ± 0.3	6.10 ± 0.4	51.26 ± 3.0
6j	>100	>100	92.78 ± 4.8	87.46 ± 4.5	57.49 ± 3.3
6k	38.35 ± 2.3	17.42 ± 1.2	19.02 ± 1.4	26.54 ± 1.8	84.58 ± 4.5
6l	55.13 ± 3.2	36.01 ± 2.2	31.89 ± 2.1	41.53 ± 2.3	25.20 ± 1.8
6m	>100	>100	>100	>100	>100
6n	>100	91.60 ± 4.7	69.53 ± 3.6	84.29 ± 4.2	16.49 ± 1.3
6o	80.36 ± 4.0	73.26 ± 3.7	55.56 ± 3.1	63.01 ± 3.2	19.98 ± 1.5
6p	28.91 ± 1.8	33.57 ± 2.1	25.69 ± 1.8	39.16 ± 2.1	49.26 ± 2.8
6q	7.49 ± 0.5	9.85 ± 0.7	5.04 ± 0.4	11.62 ± 0.8	37.04 ± 2.4
6r	26.16 ± 1.6	29.38 ± 1.8	19.64 ± 1.5	22.91 ± 1.5	72.08 ± 4.1
6s	43.02 ± 2.4	47.36 ± 2.6	36.52 ± 2.2	40.95 ± 2.3	34.90 ± 2.2
6t	37.70 ± 2.2	42.89 ± 2.4	29.81 ± 1.9	34.22 ± 2.0	>100
6u	>100	>100	89.79 ± 4.5	>100	61.19 ± 3.6
6v	67.51 ± 3.8	18.67 ± 1.3	12.23 ± 1.0	6.49 ± 0.3	58.45 ± 3.8
6w	85.75 ± 4.3	83.72 ± 4.0	68.13 ± 3.7	73.86 ± 3.8	27.85 ± 1.8
6x	>100	>100	78.36 ± 4.0	93.56 ± 4.8	>100
6y	92.14 ± 4.8	78.52 ± 3.9	61.38 ± 3.4	68.53 ± 3.5	>100
6z	20.38 ± 1.4	24.19 ± 1.7	16.78 ± 1.3	28.03 ± 1.7	65.61 ± 3.9
7a	31.17 ± 2.1	13.91 ± 1.0	10.23 ± 0.8	21.72 ± 1.4	66.09 ± 3.6
7b	52.16 ± 2.8	59.80 ± 3.3	45.67 ± 2.5	48.73 ± 2.7	31.54 ± 2.1
8a	48.24 ± 2.8	67.86 ± 3.8	43.91 ± 2.5	34.61 ± 2.1	>100
8b	14.77 ± 1.1	13.26 ± 1.1	9.98 ± 0.6	17.80 ± 1.3	56.21 ± 3.2
doxorubicin	5.23 ± 0.3	4.50 ± 0.2	5.57 ± 0.4	4.17 ± 0.2	6.72 ± 0.5
dasatinib	58.61 ± 3.4	60.84 ± 3.6	53.86 ± 3.1	46.83 ± 2.5	28.62 ± 2.1

(8a and 8b). The synthesis of 2-(2-(1*H*-indole-2-carboxamido)thiazol-4-yl)acetic acid (**7a** and **7b**) involved the conversion of ethyl 2-(2-(1*H*-indole-2-carboxamido)-thiazol-4-yl)acetate (**3a** and **3b**) using a refluxing condition with 10% NaOH. This transformation resulted in the formation of the desired product, 2-(2-(1*H*-indole-2-carboxamido)thiazol-4-yl)acetic acid (**7a/b**). The reaction conditions ensured efficient hydrolysis of the ester group, leading to the formation of the carboxylic acid derivatives. This step was crucial in obtaining the desired target compounds. Concurrently, another transformation was carried out to synthesize *N*-(4-(2-(hydroxyamino)-2-oxoethyl)thiazol-2-yl)-1*H*-indole-2-carboxamide (**8a/b**) from the starting material ethyl 2-(2-(1*H*-indole-2-carboxamido)thiazol-4-yl)acetate (**3a/b**). This conversion involved the treatment of (**3a/b**) with freshly prepared hydroxylamine (NH_2OH). The reaction proceeded efficiently, resulting in the formation of *N*-(4-(2-(hydroxyamino)-2-oxoethyl)thiazol-2-yl)-1*H*-indole-2-carboxamide (**8a/b**) in good yield. This step introduced a hydroxylamino group into the molecule, which expanded the chemical diversity and potential biological activities of the synthesized compounds (Scheme 2).

The structures of the synthesized compounds (**3**−**8**) were confirmed through analysis of their IR, mass, and NMR

https://doi.org/10.1021/acsomega.4c06889
ACS Omega 2024, 9, 41944−41967

Table 2. *In Vitro* Protein Kinase Inhibition Assay of Most Active Compounds from 6e, 6i, 6q, 6v, 7a, and 7b against EGFR, Her2, VEGFR-2, and CDK2

	in vitro protein kinase inhibition IC_{50} (μM)			
compound	EGFR	HER2	VEGFR-2	CDK2
6e	0.154 ± 0.02	0.117 ± 0.005	0.182 ± 0.008	0.357 ± 0.01
6i	0.063 ± 0.02	0.054 ± 0.002	0.119 ± 0.005	0.448 ± 0.02
6q	0.394 ± 0.03	0.779 ± 0.003	1.035 ± 0.043	1.343 ± 0.05
6v	0.081 ± 0.015	0.065 ± 0.003	0.429 ± 0.018	0.506 ± 0.02
7a	0.618 ± 0.04	0.618 ± 0.008	1.212 ± 0.05	1.711 ± 0.07
7b	1.744 ± 0.02	1.774 ± 0.003	0.921 ± 0.08	3.191 ± 0.12
dasatinib	0.126 ± 0.01	0.040 ± 0.002	0.188 ± 0.049	0.651 ± 0.03
gefitinib	0.042 ± 0.002			
lapatenib		0.0543 ± 0.002		
sorafenib			0.049 ± 0.002	
roscovetine				0.834 ± 0.03

spectral data. The observed characteristic IR bands, proton peaks and mass spectral data supported the elucidation of the structures of the final products (Please see the Supporting Information for the spectra).

Biological Evaluation of 6−8. *In Vitro Cytotoxicity Assay of 6−8.* A comprehensive *in vitro* cytotoxicity evaluation was conducted for the synthesized compounds **6a−6z**, **7a**, **7b**, **8a**, and **8b** to assess their cytotoxic potential using the widely accepted MTT method. Multiple cancer cell lines, including human colorectal carcinoma (HCT-116), hepatocellular carcinoma (HepG2), epithelioid cervix carcinoma (HeLa), and breast cancer (MCF-7) cell lines, were employed for this purpose. Additionally, the toxicity of these compounds on normal cell lines was examined using a noncancerous diploid human cell line composed of fibroblasts derived from lung tissue (WI-38). The resulting data, presented in Table 1, represents the concentration at which 50% of cell death (IC_{50} values) occurred and was compared to the cytotoxicity of dasatinib and doxorubicin well-known anticancer agents. Remarkably, the synthesized compounds exhibited a diverse range of cytotoxic effects. Compound **6a** with free benzylidene group shows moderate IC_{50} values (37.25−65.37 μM) against four cancer cell lines, and interestingly, it also was active against the normal cell line WI-38, with an IC_{50} of 18.21 μM. Although the IC_{50} of **6a** is lower than that of doxorubicin (4.17−5.57 μM), it is comparable to the dasatinib (46.83−60.84 μM). Inserting various substituents, such as compounds **6b** (4-Br), **6c** (4-Cl), **6d** (4-F), **6f** (2-OCH_3), **6g** (4-OCH_3) and **6b** (4-SCH_3) did not improve the IC_{50} compared to **6a**, as all of these compounds showed IC_{50} values between 59.22 and >100 μM. On the other hand, the insertion of a nitro group at the 4-position, as seen in compounds **6h** (4-NO_2), 6k (2-OH and 4-OCH_3), and **6l** (naphthyl), showed improved IC_{50} values, ranging from 17.42 to 55.13 μM. These values are even better than the dasatinib. However, compound **6e**, with a hydroxy group at the 4-position, and **6i**, featuring a dimethylamine group at the 4-position, demonstrated potent cytotoxicity against the tested cell lines, with IC_{50} values between 4.36 and 23.86 μM, except against HepG2 cells (32.74−69.63 μM). Interestingly, **6e** and **6i** also exhibited excellent selectivity toward the normal WI-38 cell line, with IC_{50} values of 51.26−71.90 μM, which are much higher than the values for doxorubicin (6.72 μM) and dasatinib (28.62 μM). Compounds with a methoxy group on the indole moiety (**6m−6z**) also displayed similar results as **6a−6l**. Compound **6m**, with a free benzylidene group and a methoxy group at the 5-position of the indole, shows IC_{50} values greater than 100 μM against all five cancer/noncancer cell lines. Inserting various substituents, compounds **6n** (4-Br), **6r** (4-Cl), **6s** (4-NO_2), **6w** (4-SCH_3), **6x** (3,4-di-Cl), and **6y** (2-OH and 4-OCH_3) improved the IC_{50} values compared to **6m**, but they are still lower than dasatinib, with IC_{50} values ranging from 55.56 to >100 μM. On the other hand, the introduction of substituents in compounds **6p** (4-F), **6r** (4-CH_3), **6s** (2-OCH_3), **6t** (4-OCH_3), and **6z** (naphthyl) improved the IC_{50} values to be better than dasatinib, and some were even comparable to doxorubicin, with IC_{50} values ranging from 16.78 to 47.36 μM. As expected, compounds **6q** and **6v**, with a hydroxy group at the 4-position and a dimethylamine group at the 4-position, similar to **6e** and **6i**, demonstrated potent cytotoxicity against the tested cell lines, with IC_{50} values between 5.04 and 18.67 μM, except for compound **6v** against HCT-116 cells (67.51 μM). Interestingly, compounds **6v** and **6w** also exhibited excellent selectivity toward the normal WI-38 cell line, with IC_{50} values of 37.4 and 58.45 μM, respectively. Compound **7** and **8** also showed comparable IC_{50} values as dasatinib. Their cytotoxic effects were particularly noteworthy, indicating their potential as effective therapeutic options. These findings highlight the significance of structural modifications in designing novel compounds with potent cytotoxic properties. The presence of specific functional groups, such as the dimethyl amine group, played a crucial role in enhancing the cytotoxicity of the synthesized compounds. These results pave the way for further exploration and optimization of these compounds as potential anticancer agents. It is important to note that the comprehensive *in vitro* cytotoxicity evaluation also considered the toxicity of the synthesized compounds on normal cell lines. This assessment revealed the potential selectivity and specificity of the compounds toward cancer cells, as they exhibited varying degrees of cytotoxic effects while maintaining a relatively lower impact on the noncancerous WI-38 cell line. This aspect is crucial in the development of anticancer drugs, as minimizing harm to normal cells is a critical objective. The tested compounds demonstrate significant antiproliferative activity across multiple cancer cell lines, though not as potent as doxorubicin. Their structural differences suggest potential for novel modes of action, which could be advantageous. Several compounds exhibit IC_{50} values comparable or better than dasatinib, indicating shared or complementary mechanisms. The diversity of the compounds provides opportunities to explore structure−activity relationships and identify new lead

https://doi.org/10.1021/acsomega.4c06889
ACS Omega 2024, 9, 41944−41967

candidates. While not as potent as the reference drugs, the tested compounds still show promise as potential anticancer agents worthy of further optimization and development.

*In Vitro Tyrosine Kinase Inhibition Assays of **6e, 6i, 6q, 6v, 7a, and 7b**.* To understand the molecular mechanism underling the cytotoxic effects of compounds the series, the six most active compounds (**6e**, **6i**, **6q**, **6v**, **7a**, and **7b**) were further assessed for testing the enzymatic activities against EGFR, Her2, VEGFR-2 and cyclin-dependent kinase 2 (CDK2) kinase enzymes (Table 2). Dasatinib was used as a reference standard for all tested kinases, along with other well-known inhibitors (gefitinib for EGFR, lapatinib for Her2, sorafenib for VEGFR-2 and roscovitine for CDK2). Results in Table 2 showed that compounds **6i** and **6v** were able to successfully inhibit the four investigated protein kinases in similar potencies to dasatinib and the selected reference kinase inhibitors. Compound **6i** demonstrates potent inhibition of EGFR with an IC_{50} of 0.063 μM, as well as Her2 with an IC_{50} of 0.054 μM. It also exhibits significant inhibition of VEGFR-2 with an IC_{50} of 0.119 μM and CDK2 with an IC_{50} of 0.448 μM. Compound **6v** shows potent inhibition of EGFR (IC_{50} = 0.081 μM) and Her2 (IC_{50} = 0.065 μM), along with significant inhibition of VEGFR-2 (IC_{50} = 0.429 μM) and CDK2 (IC_{50} = 0.506 μM). Compounds **6e** and **6q** exhibited moderate protein kinase inhibition activities, while compounds **7a** and **7b** demonstrated weak potency. In brief, Compound **6e** displays notable inhibition of EGFR (IC_{50} = 0.154 μM), Her2 (IC_{50} = 0.117 μM), VEGFR-2 (IC_{50} = 0.182 μM), and CDK2 (IC_{50} = 0.357 μM) and compound **6q** exhibits moderate inhibition of EGFR (IC_{50} = 0.394 μM), substantial inhibition of Her2 (IC_{50} = 0.779 μM), and significant inhibition of VEGFR-2 (IC_{50} = 1.035 μM) and CDK2 (IC_{50} = 1.343 μM). The presence of a dimethylamine group at the 4-position appears to be a favorable structural feature for the potent inhibition of multiple kinases, as evidenced by the strong activities of compounds **6i** and **6v**. The dimethylamine substituent likely contributes to enhanced binding interactions within the active sites of EGFR, HER2, VEGFR-2, and CDK2, leading to the potent inhibitory effects observed for these two compounds. The tested compounds (**6e**, **6i**, **6q**, **6v**, **7a** and **7b**) and the reference kinase inhibitors (Dasatinib, Gefitinib, Lapatinib, Sorafenib, Roscovitine) share common structural features that contribute to their observed protein kinase inhibition activities. These include heterocyclic scaffolds, heteroaryl substituents, and the presence of halogens or other lipophilic groups, which facilitate key binding interactions within the kinase active sites. Additionally, hydrogen bond donor and acceptor functionalities allow for the formation of crucial hydrogen bonding interactions. These structural similarities suggest the tested compounds and references may share common binding modes and mechanisms of action, targeting the ATP-binding pockets or other critical regions of kinases like EGFR, HER2, VEGFR-2, and CDK2. The specific substituents, such as the dimethylamine group in compounds **6i** and **6v**, can further enhance binding affinity and selectivity toward particular kinases, as evident from their potent inhibitory activities.

Cell Cycle Analysis of Most Active Compounds 6i and 6v. In order to examine how the synthesized compounds impact cell cycle progression, MCF-7 cells were exposed to compounds **6i** and **6v** at their respective IC_{50} values for 24 h (Table 3). Following treatment, the cells were stained with propidium iodide (PI) and subjected to flow cytometry analysis to determine the distribution of cell cycle phases.

Table 3. Results of Cell Cycle Analysis of MCF-7 Cells Treated with Compounds 6i and 6v

	DNA content (%)		
compound/cell line	%G0/G1	%S	%G2/M
Cont. MCF-7	63.41	23.96	12.63
6i/MCF-7	55.18	21.22	23.6
6v/MCF-7	51.99	18.43	29.58

Results presented in Table 3 and Figure 3 illustrate the cell cycle analysis on MCF-7 cells treated with compounds **6i** and **6v**, compared to the control group, show a decrease in the percentage of cells in the G0/G1 phase and an increase in the percentage of cells in the G2/M phase for both compounds. These findings suggest an effect of compounds **6i** and **6v** on promoting cell cycle progression in MCF-7 cells. In brief, the analysis involved measuring the percentage of cells in different phases of the cell cycle: G0/G1 (resting phase), S (DNA synthesis phase), and G2/M (preparation for cell division phase). In the control group of MCF-7 cells, 63.41% of the cells were found to be in the G0/G1 phase, indicating a significant proportion of cells in the resting state. Approximately 23.96% of the cells were in the S phase, where DNA synthesis occurs, and 12.63% of the cells were in the G2/M phase, preparing for cell division. When MCF-7 cells were treated with compound **6i**, there was a decrease in the percentage of cells in the G0/G1 phase to 55.18%. This suggests that compound **6i** may induce cell cycle progression and reduce the number of cells in the resting state. The percentage of cells in the S phase remained relatively similar at 21.22%, while there was a significant increase in the percentage of cells in the G2/M phase to 23.6%. Similarly, treatment with compound **6v** resulted in a further decrease in the percentage of cells in the G0/G1 phase to 51.99%. This indicates a stronger effect in promoting cell cycle progression compared to compound **6i**. The percentage of cells in the S phase decreased to 18.43%, while there was a substantial increase in the percentage of cells in the G2/M phase to 29.58%. These findings suggest that both compounds **6i** and **6v** have an impact on cell cycle progression in MCF-7 cells. They appear to induce a shift from the G0/G1 phase toward the G2/M phase, potentially affecting cell proliferation and division.

Apoptosis Analysis of Compounds 6i and 6v. *Annexin-V/Propidium Iodide (PI) Staining Assay of Compounds **6i** and **6v**.* Table 4 presents the results of apoptotic cell distribution analysis conducted on MCF-7 cells treated with compounds **6i** and **6v**, along with a control group. The analysis involved categorizing the cells into three categories: total apoptosis, early apoptosis, and late apoptosis, as well as measuring necrosis. In the control group of MCF-7 cells, the total percentage of apoptotic cells was 2.46%. Within this, 0.51% were in the early apoptotic stage, and 0.22% were in the late apoptotic stage. The majority of the cells (1.73%) did not show signs of apoptosis and were considered nonapoptotic. When MCF-7 cells were treated with compound **6i**, there was a significant increase in apoptosis. The total percentage of apoptotic cells rose to 29.75%, with 14.59% in the early apoptotic stage and 9.03% in the late apoptotic stage. Additionally, 6.13% of the cells exhibited necrotic characteristics (Table 4 and Figure 4). Similarly, treatment with compound **6v** resulted in a further increase in apoptosis. The total percentage of apoptotic cells reached 35.11%, with 11.63% in the early apoptotic stage and 18.66% in the late

https://doi.org/10.1021/acsomega.4c06889
ACS Omega 2024, 9, 41944−41967

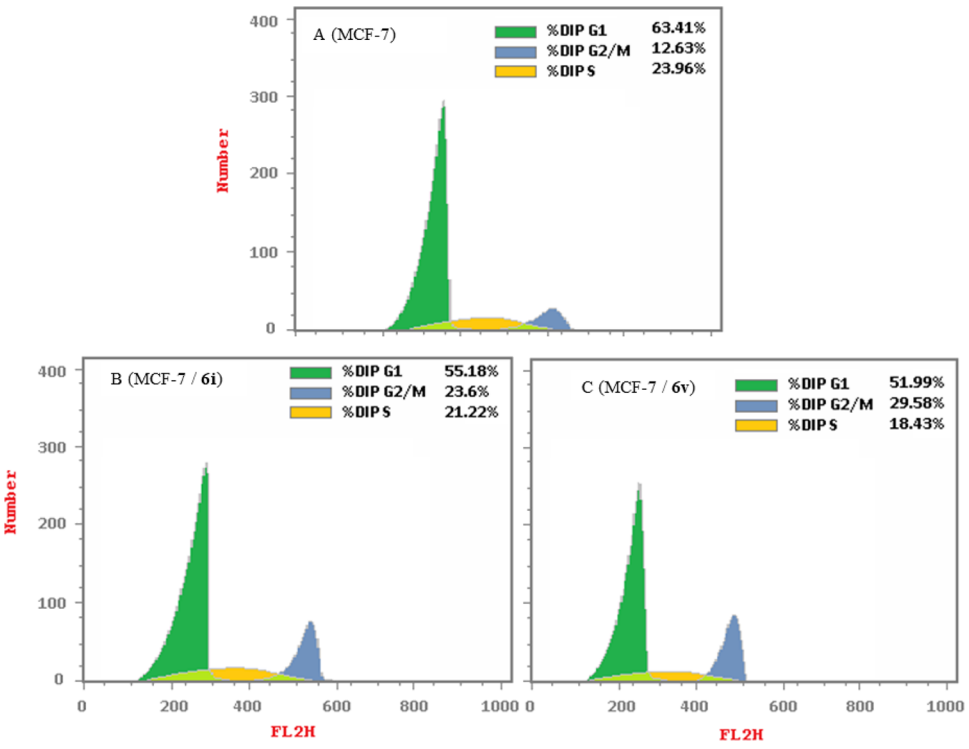

Figure 3. Cell cycle phases of MCF-7 cells. (A) Only cell lines without a compound; (B) treatment with compound **6i**; and (C) treatment with compound **6v**.

Table 4. Results of Apoptotic Cell Distribution of MCF-7 Cells Treated with Compounds 6i and 6v

	apoptosis (% of apoptotic cell lines)			
sample	alive cells	early	late	necrosis
Cont. MCF-7	97.54	0.51	0.22	1.73
6i/MCF-7	70.25	14.59	9.03	6.13
6v/MCF-7	64.89	11.63	18.66	4.82

apoptotic stage. The percentage of cells showing necrosis was 4.82%. These findings indicate that both compounds **6i** and **6v** induce apoptosis in MCF-7 cells. Compound **6v** appears to have a stronger effect, leading to a higher percentage of apoptotic cells compared to compound **6i**. The increase in apoptotic cell distribution suggests that these compounds may have potential anticancer effects by promoting programmed cell death in MCF-7 cells. The presence of necrosis in addition to apoptosis in MCF-7 cells treated with compounds **6i** and **6v** raises interesting implications for their cellular effects. Necrosis is a form of cell death characterized by cellular swelling, rupture, and inflammation, often associated with cellular damage or stress. The observed percentages of cells exhibiting necrosis in the experimental groups suggest that the compounds may induce cytotoxic effects beyond apoptosis alone. The induction of necrosis could be attributed to the compounds' potential disruption of cellular homeostasis, leading to cell membrane damage and subsequent release of intracellular contents. Further investigations into the underlying mechanisms of necrosis induction by compounds **6i** and **6v** would be valuable to better understand their overall impact on cell fate and to assess the potential therapeutic significance of these compounds in cancer treatment.

Determination of Apoptotic Protein Levels of Compounds 6i and 6v. Table 5 displays the results of RT-PCR fold change analysis, which measures the relative expression levels of various apoptotic proteins in MCF-7 cells following treatment with compounds **6i** and **6v**, compared to the control group. A fold change value of 1 indicates no change in expression compared to the control. In MCF-7 cells treated with compound **6i**, there is a significant increase in the expression of Bax (7.0308-fold), p53 (5.2183-fold), cyc (6.0196-fold), casp7 (5.5872-fold), casp8 (3.7313-fold), and casp9 (9.2404-fold). These proteins are known to promote apoptosis. On the other hand, the expression of the antiapoptotic proteins Bcl-2 and Her2 shows a decrease, with fold change values of 0.209 and 0.4601, respectively. Similarly, in MCF-7 cells treated with compound **6v**, there is an increase in the expression of Bax (4.1987-fold), p53 (6.2095-fold), cyc (4.0957-fold), casp7 (3.5504-fold), casp8 (2.0811-fold), and casp9 (6.7736-fold). The expression of Bcl-2 and Her2 also decreases, with fold change values of 0.2647 and 0.5753, respectively. In the control group, the expression levels of all the apoptotic proteins are considered as the baseline, with fold change values of 1. These results indicate that both compounds **6i** and **6v** can modulate the expression of various apoptotic proteins in MCF-7 cells. The upregulation of pro-apoptotic proteins (Bax, p53, cyc, casp7, casp8, casp9) and down-regulation of antiapoptotic proteins (Bcl-2, Her2) suggest the potential of these compounds to induce apoptosis and promote cell death in MCF-7 cells. These findings provide insights into the molecular mechanisms underlying the apoptotic effects of compounds **6i** and **6v** and suggest their potential as therapeutic agents for targeting apoptosis-related pathways in cancer cells.

In Silico Studies of the Synthesized Compounds 3−8. *Analysis of the Binding Mechanism of Compounds **6i** and **6v** and Reference Compounds by Molecular Docking Study.* The importance of docking in comparing the results with *in*

https://doi.org/10.1021/acsomega.4c06889
ACS Omega 2024, 9, 41944−41967

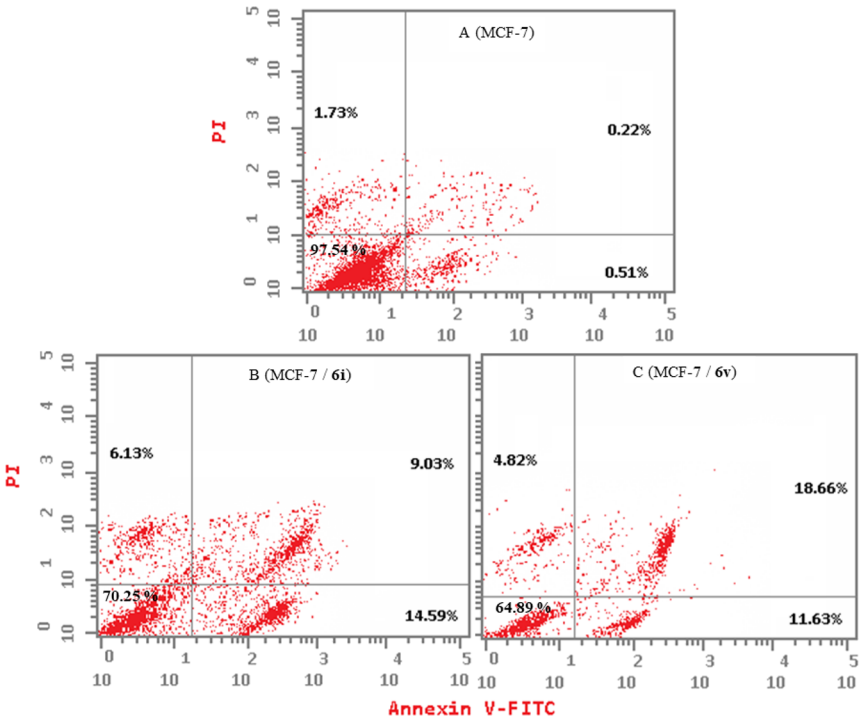

Figure 4. Apoptotic cell distribution of MCF-7 cells: (A) control-without compounds, cell lines only; (B) treatment with compound **6i**; and (C) treatment with compound **6v**.

Table 5. RT-PCR Fold Change for Apoptotic Protein following Treatment with 6i and 6v

	RT-PCR fold change							
Samples	Bax	Bcl-2	p53	Her2	cyc	casp7	casp8	casp9
6i/ MCF-7	7.0308	0.209	5.2183	0.4601	6.0196	5.5872	3.7313	9.2404
6v/ MCF-7	4.1987	0.2647	6.2095	0.5753	4.0957	3.5504	2.0811	6.7736
control MCF-7	1	1	1	1	1	1	1	1

Table 6. Binding Affinity, Interacting Residues, and Types of Interactions Mediated by Compounds 6i and 6v and Reference Compounds

	binding affinity (kcal/mol)				hydrogen bonds			
entry	EGFR	HER2	VEGFR2	CDK2	EGFR	HER2	VEGFR2	CDK2
6i	−8.9	−9.5	−9.6	−8.3	Cys797, Lys745	Asp808, Asn850, Arg849	Asp1046, Glu885	Glu12, Asp86
6v	−8.3	−8.7	−9.5	−8.1	Lys745	Ser728	Asp1046	Gln131, Glu12, Lys33
gefitinib	−8.4							
lapatinib		−10.4				Met801, Ser728		
sorafenib			−10.7				Glu885, Asp1046, Cys919	
roscovitine				−8.2				Gln131, Asp145
dasatinib	−8.0	−9.5	−8.1	−8.4	Asp855, Ser720	Asp863, Leu726, Asp808	Asp1046	His84, Lys129, Lys33, Asp145

vitro biological activity lies in its ability to provide a molecular-level understanding of the binding interactions between the compounds and the target receptors. Docking simulations enable the exploration of potential binding modes and the estimation of binding affinities, offering valuable insights into the molecular mechanisms underlying the observed biological effects. By combining the results of docking studies with experimental *in vitro* biological activity data, we can establish a correlation between the predicted binding interactions and the observed biological responses. This comparison allows us to validate the reliability and accuracy of the docking predictions, strengthening our confidence in the predicted drug-receptor interactions. Moreover, docking studies enable the identification of key residues involved in the binding interactions, which can guide the design and optimization of more potent and selective compounds. This knowledge aids in the development of novel therapeutics with improved efficacy and reduced off-target effects. Docking studies play a crucial role in elucidating the biological activity of compounds and predicting their interactions with target receptors. By comparing the docking results with *In-vitro* biological activity data, we can validate the computational predictions and gain deeper insights into the molecular basis of the observed biological effects. This integrated approach enhances our understanding of the structure−activity relationships and facilitates the rational design of effective drugs. In order to gain insights into the biological activity of the synthesized compounds and to predict their interactions with target

https://doi.org/10.1021/acsomega.4c06889
ACS Omega 2024, 9, 41944−41967

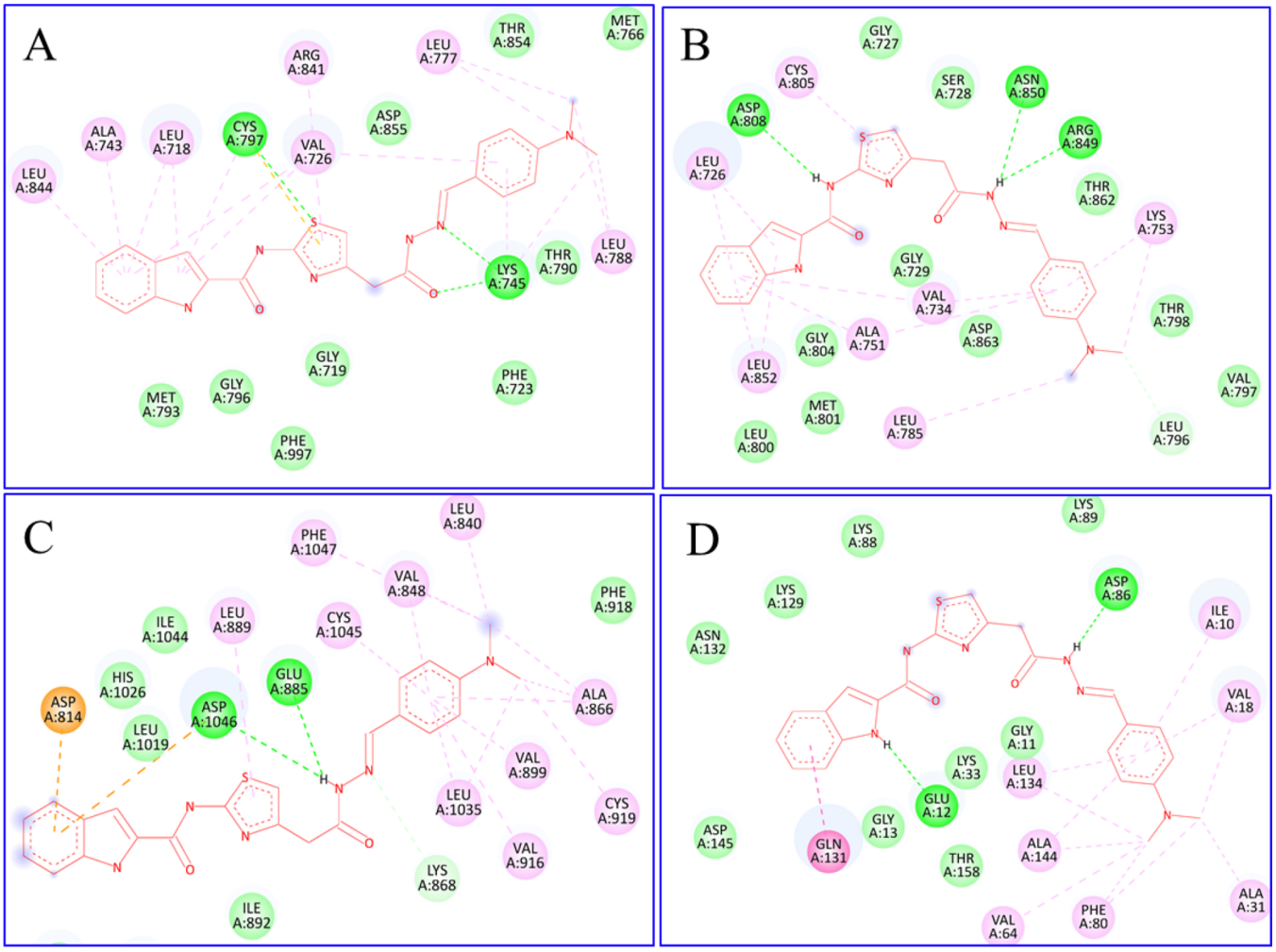

Figure 5. Intermolecular interaction between compound **6i** and enzymes with (A) EGFR, (B) HER2, (C) VEGFR2, and (D) CDK2.

receptors, a comprehensive docking study was conducted. Specifically, compounds **6i** and **6v** were meticulously docked into the active sites of EGFR, HER2, VEGFR2, and CDK2. To establish a reference point, cocrystal ligands gefitinib, lapatinib, sorafenib and roscovitine were utilized as standards for each respective target. Additionally, the structurally similar dasatinib was docked alongside our synthesized compounds (**6i** and **6v**) for comparison (Table 6).

Regarding EGFR, dasatinib binds within the ATP binding pocket of the catalytic tyrosine kinase domain, competing with ATP. The docking analysis of compounds **6i** and **6v** with EGFR kinase are shown in Table 6 and Figures 5 and 6. Both compounds revealed several van der Waals and multiple hydrophobic interactions (Table S3 and Figure S1). In contrast, Gefitinib did not form any hydrogen bond but displayed hydrophobic and van der Waals interactions. The study identified interactions with DFG motif residues and ATP binding site residues, including Asp855 and Phe856, as the primary inhibitory mechanisms against EGFR kinase.[101] The docking results demonstrated that both compounds **6i** and **6v** exhibited van der Waals interactions with ASP855 of the DFG motif residue. However, the reference compounds gefitinib and dasatinib showed hydrophobic interactions with ASP855 and PHE856 of the DFG motif, respectively. The binding affinities for gefitinib, compound **6i**, compound **6v**, and dasatinib with EGFR were −8.4, −8.9, −8.3, and −8.0 kcal/mol, respectively (Table 6). Thus, the synthesized compounds have the potential to bind to the ATP binding pocket and inhibit EGFR kinase activity (Figure S2).

When overexpressed, human epidermal growth factor receptor-2 (HER2), a membrane tyrosine kinase, can significantly impact cell survival and proliferation.[102,103] Important amino acids in the ATP binding pocket of HER2 have been identified, including LYS753, VAL734, ALA751, GLN799, MET801, LEU852, LEU726, PHE1004, ASP863, ASN850, GLU770, MET774, LEU785, and LEU796. In the case of synthesized compound **6i**, it formed three hydrogen bonds with ASP808, ASN850, and ARG849 residues (Table 6 and Figure 5). Additionally, it exhibited hydrophobic interactions with LEU726, VAL734, ALA751, LEU852, LEU785, and LYS753. van der Waals interactions were observed with MET801 and ASP863, which are important residues for ATP binding (Table S4). Compound **6v**, on the other hand, formed one hydrogen bond with SER728 (Table 6 and Figure 6) and demonstrated hydrophobic interactions with key residues for the ATP binding site, namely VAL734, LEU852, LEU726, LEU796, LEU785, and MET774 (Table S4 and Figure S3). It also displayed van der Waals interactions with ASN850, ALA751, LYS753, and GLU770, which are considered key residues in the active site of the kinase. The reference compounds lapatinib and dasatinib showed similar interactions with the ATP binding pocket (Figure S4).

https://doi.org/10.1021/acsomega.4c06889
ACS Omega 2024, 9, 41944−41967

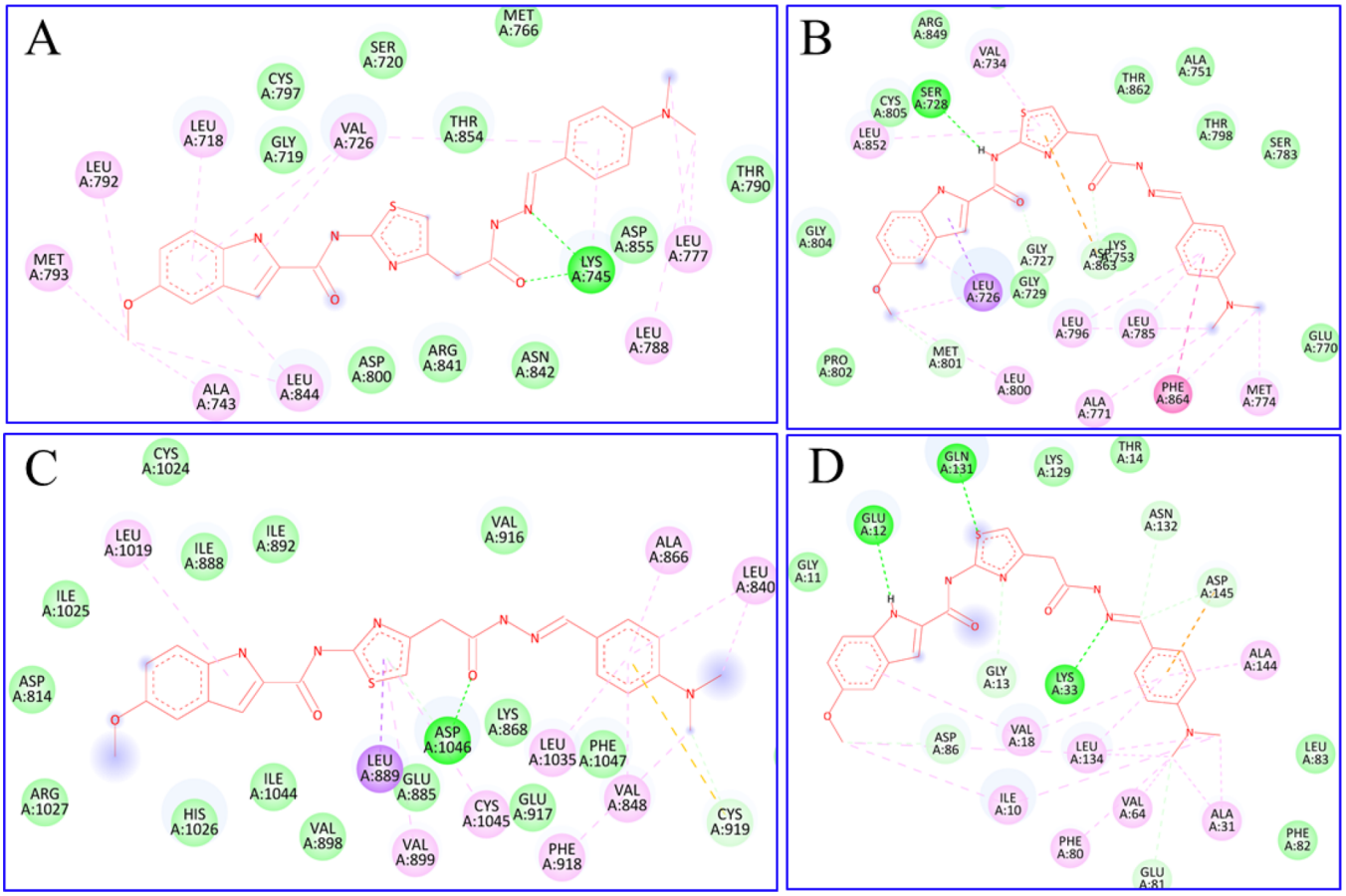

Figure 6. Intermolecular interaction between compound **6v** and enzymes: (A) with EGFR; (B) with HER2; (C) with VEGFR2; and (D) with CDK2.

Consequently, compound **6i** and compound **6v** have the potential to compete with ATP for the binding pocket and effectively inhibit HER2 (Figures S3 and S4). The binding affinities for lapatinib, dasatinib, compound **6i**, and compound **6v** with HER2 were calculated as −10.4, −9.5, −9.5, and −8.7 kcal/mol, respectively (Table 6). It is worth noting that dasatinib and compound **6i** exhibited similar binding affinities.

It has been established that Vascular Endothelial Growth Factor Receptor 2 (VEGFR2 or KDR) plays a crucial role in regulating tumor angiogenesis through VEGF signaling.[104−107] Structural analysis of VEGFR2 kinase bound with an inhibitory compound has identified key residues in the ATP binding site, namely CYS919 in the hinge region, Glu885 in the αC helix, and Asp1046 in the DFG loop.[108] In the case of synthesized compound **6i**, it formed a hydrogen bond with ASP1046 of the DFG loop and GLU885 of the αC helix (Table 6 and Figure 5). Additionally, it exhibited hydrophobic interactions and with CYS919 in the hinge region. Compound **6v**, on the other hand, formed one hydrogen bond with ASP1046 and showed hydrophobic interaction with CYS919, along with van der Waals interactions with GLU885 (Table S5 and Figure S5). Sorafenib, another compound, formed three hydrogen bonds with Glu885, Asp1046, and Cys919. Dasatinib, on the other hand, was stabilized by a hydrogen bond with ASP1046 and a hydrophobic interaction with Cys919. Therefore, both compound **6i** and compound **6v** interacted with all the key residues. Consequently, compounds **6i** and **6v** have the potential to bind to the active site of VEGFR2 kinase and act as inhibitors of VEGFR2 kinase activity (Figure S6). The binding affinities for sorafenib, dasatinib, compound **6i**, and compound **6v** with VEGFR2 kinase were calculated as −10.7, −8.1, −9.6, and −9.5 kcal/mol, respectively (Table 6). These results indicate that sorafenib has a higher binding affinity than the studied compounds on the active site. Interestingly, synthesized compounds **6i** and **6v** shows higher binding affinity than the dasatinib on the active site.

The primary role of Cyclin-Dependent Kinase 2 (CDK2) is to regulate the progression of the cell cycle. This member of the Cyclin-Dependent Kinase (CDK) family is involved in modulating G2 progression, G1/S phase transition, and DNA synthesis.[109] A study has shown that Roscovitine acts as an ATP competitive inhibitor by binding to the ATP binding region of CDK2.[110] Therefore, we utilized the CDK2-ATP complex (PDB ID: 1HCK) for further analysis. Docking analysis of compound **6i** and **6v** with CDK2 were given in Table 6 and Figures 5 and 6. The reference compound roscovitine formed three hydrogen bonds with Gln131 and Asp145, while dasatinib formed four hydrogen bonds with His84, Lys129, Lys33, and Asp145. By examining the structure of the CDK2-ATP complex (PDB ID: 1HCK),[111] it was evident that important residues for binding to the ATP binding site through hydrogen bonds include THR14, ASP86, GLN131, GLU81, and LEU83 (Table S6 and Figure S7). The compounds **6i** and **6v** exhibited hydrophobic interactions along with some with van der Waals interactions. Interestingly, our studied compounds did not form hydrogen bonds with these crucial binding site residues but were stabilized by different interaction patterns. Therefore, both compound **6i**

https://doi.org/10.1021/acsomega.4c06889
ACS Omega 2024, 9, 41944−41967

Table 7. Analysis of Drug Likeness and Pharmacokinetic Properties by QikProp for the Synthesized Compounds and Dasatinib

no.	MW[a]	HBD[b]	HBA[c]	QlogPo/w[d]	QPlogS[e]	QPlogHERG[f]	QPPCaco[g]	QPlogBB[h]	QPPMDCK[i]	HOA(%)[j]
6a	403	3	6.5	3.982	−6.360	−7.737	432.866	−1.380	392.509	100
6b	482	3	6.5	4.542	−7.184	−7.635	423.535	−1.225	1041.11	100
6c	437	3	6.5	4.467	−7.080	−7.620	433.096	−1.234	967.969	100
6d	421	3	6.5	4.214	−6.716	−7.601	433.137	−1.277	708.743	100
6e	419	4	7.25	3.253	−6.190	−7.736	137.378	−2.115	112.682	84
6f	433	3	7.25	4.118	−6.779	−7.776	436.840	−1.509	393.430	100
6g	433	3	7.52	4.047	−6.466	−7.507	452.671	−1.432	408.890	100
6h	448	3	7.5	3.321	−6.672	−7.740	55.368	−2.650	42.196	77
6i	446	3	7.5	4.54	−7.540	−7.860	421.491	−1.586	378.421	100
6j	449	3	7	4.448	−7.141	−7.627	357.602	−1.524	475.251	100
6k	449	4	8	3.311	−6.240	−7.505	155.483	−2.117	128.816	85
6l	453	3	6.5	4.808	−7.279	−8.125	429.343	−1.412	389.058	100
6m	433	3	7.25	4.07	−6.674	−7.689	437.047	−1.493	394.461	100
6n	512	3	7.25	4.630	−7.498	−7.579	437.722	−1.337	1046.287	88
6o	467	3	7.25	4.555	−7.395	−7.565	437.279	−1.347	972.783	100
6p	451	3	7.25	4.302	−7.031	−7.550	437.320	−1.390	712.268	100
6q	449	4	8	3.305	−6.360	−7.541	131.875	−2.229	108.032	84
6r	447	3	7.25	4.360	−7.208	−7.547	437.047	−1.530	394.461	100
6s	463	3	8	4.207	−6.776	−7.488	523.412	−1.463	479.893	100
6t	463	3	8	4.109	−6.772	−7.449	443.117	−1.562	399.571	100
6u	478	3	8.25	3.365	−6.824	−7.544	53.150	−2.772	40.455	64
6v	476	3	8.25	4.656	−7.336	−7.465	659.162	−1.360	613.786	100
6w	479	3	7.75	4.639	−7.482	−7.509	428.828	−1.497	696.417	100
6x	502	3	7.25	4.944	−7.828	−7.311	426.747	−1.203	1976.765	90
6y	479	4	8.75	3.236	−6.157	−7.206	132.518	−2.285	90.680	83
6z	483	3	7.25	4.767	−7.436	−8.055	357.899	−1.649	265.396	100
7a	301	3	6	2.058	−3.801	−3.831	46.273	−1.333	44.537	69
7b	331	3	6.75	2.137	−3.989	−3.695	47.470	−1.418	45.784	69
8a	316	4	8.2	0.108	−2.155	−4.363	63.441	−1.580	105.103	59
8b	346	4	8.95	0.131	−2.249	−4.243	56.684	−1.722	96.954	59
D[k]	488	3	10.7	3.118	−5.590	−7.360	171.424	−0.658	291.988	85

[a]Molecular weight in Dalton (acceptable range: <500). [b]Hydrogen bond donor (acceptable range: ≤5). [c]Hydrogen bond acceptor (acceptable range: ≤10). [d]Predicted octanol/water partition coefficient (acceptable range: −2 to 6.5). [e]Predicted aqueous solubility, S in mol/dm^{-3} (acceptable range: − 6.5 to 0.5). [f]Predicted IC_{50} value for blockage of HERG K+ channels (concern: below −5); Caco-2 value, permeability to Caco-2 (human colorectal carcinoma) cells *in vitro*. [g]Blood-brain barrier permeability (acceptable range: ∼−0.4). [h]Predicted apparent MDCK cell permeability in nm/s. [i]QPPMDCK= > 500 is great, < 25 is poor. [j]Predicted human oral absorption on 0 to 100% scale (<25% is poor and >80% is high); [k]D = Dasatinib

and compound **6v** have the ability to bind to the ATP binding pocket residues of the CDK2 domain and act as ATP competitive inhibitors (Figure S8). The binding affinities for roscovitine, dasatinib, compound **6i**, and compound **6v** with CDK2 were calculated as −8.2, −8.4, −8.3, and −8.1 kcal/mol, respectively (Table 6). It is worth noting that, in the case of EGFR, despite having higher in vitro protein kinase inhibitory activity and greater binding affinity in the active site, compounds **6i** and **6v**, our reference compounds dasatinib and gefitinib, did not form any hydrogen bonds with the residues that formed hydrogen bonds with the cocrystallized ligands (Figure S9). However, they were stabilized by different interaction patterns, including hydrophobic and van der Waals interactions with those residues. Similar phenomena were observed in the docking result of compounds **6i** and **6v** with HER2. From the Tak-285-EGFR and SYR127063-HER2 complex, it was found that both formed several hydrogen bonds with the EGFR and HER2 residues, respectively. Our observation revealed that the different binding modes, inherent flexibility, conformational flexibility of our molecules, and side chain flexibility in the active site of protein led to distinct interaction patterns. In theory, in order to replicate the binding process in actual systems, a ligand should be regarded as a completely flexible body during the docking process.[112] Variations between docking results and experimentally determined binding modes, such as those visualized in cocrystallized ligands, are often because the conditions during the experimental process differed from the computational model in terms of pH, temperature, and the presence of cofactors.

In conclusion, based on the docking results, both synthesized compound **6i** and compound **6v** demonstrated better binding affinity with the target proteins compared to the reference compounds. This suggests that these synthesized compounds have the potential to act as inhibitors of VEGFR2 kinase and CDK2, respectively. However, it is important to consider that the observed differences in binding affinity may be influenced by various factors such as cellular uptake, metabolism, or off-target effects. These factors could contribute to the compounds' varying cytotoxic effects. Further investigations are required to explore the unique characteristics of the kinase pathway, the cellular environment, and the

https://doi.org/10.1021/acsomega.4c06889
ACS Omega 2024, 9, 41944−41967

downstream consequences of kinase inhibition. By gaining a deeper understanding of these aspects, we can fully comprehend the underlying mechanisms and potential therapeutic implications of synthesized compound **6i** and compound **6v**. Overall, these findings highlight the promising nature of compound **6i** and compound **6v** as potential candidates for further development as VEGFR2 kinase and CDK2 inhibitors, respectively and acts as ATP competitive inhibitors. Continued research and comprehensive studies are essential to unravel the complete picture and harness the therapeutic potential of these compounds.

***In Silico* ADME Studies of the Synthesized Compounds 6−8 and Dasatinib.** Rational drug design plays a vital role in modern drug discovery techniques. By utilizing advanced computational methods such as ADME (absorption, distribution, metabolism, and excretion) studies, which are determined through pharmacokinetics analysis, we can efficiently select effective drugs in terms of cost, time, and efficiency. Recent advancements in computational chemistry have made it more convenient to conduct ADME analysis both *in vitro* and *in vivo*, allowing the pharmaceutical industry to quickly screen a large number of compounds.[113] In this experiment, we employed an in-silico approach to predict the ADME properties of our synthesized compounds (**6−8**). Table 7 summarizes the results, with dasatinib chosen as our reference compound. Molecular weight is an important factor affecting intestinal absorption, as high molecular weight compounds tend to be less effectively absorbed through the digestive system.[114,115] Therefore, we kept the molecular weight of the synthesized compounds (**6−8**) low, with most of them showing a molecular weight lower than that of dasatinib. Except for compounds **6n** and **6x**, all of our synthesized compounds had molecular weights below 500. Furthermore, our compounds demonstrated a suitable number of hydrogen bond donors (2−5), falling within the recommended range (<5). The number of hydrogen bond acceptors in the synthesized compounds was also within the advised range, with less than 10 acceptors. In comparison, dasatinib showed a hydrogen bond donor value of 3 and a hydrogen bond acceptor value of 10.70, slightly higher than the recommended range. Thus, the synthesized compounds showed superiority over dasatinib in terms of hydrogen bond acceptor values. In 2002, Jorgensen and Duffy developed a parameter to evaluate a drug's bioavailability using the octanol/water partition coefficient and solubility score. The acceptable range for the octanol/water partition coefficient is −2 to 6.5, and for solubility scoring, it is −6.5 to 0.5 mol/dm^{-3}.[116] The octanol/water partition coefficient of our synthesized compounds (**6−8**) falls within this range (0.108−4.944), similar to dasatinib. However, the solubility score of some of the synthesized compounds is slightly lower than the reference value, while dasatinib demonstrated better solubility. Regarding the predicted log IC_{50} values (logHERG) for HERG K+ channel blockage, values greater than −5 are considered preferable, as blocking HERG K+ channels can have negative effects on the heart.[117] Four of our synthesized compounds (**7** and **8**) showed preferred values. However, dasatinib and some of our designed molecules exhibited lower values, less than −5. The Caco-2 cell is considered the most accurate *In-vitro* model for estimating transdermal delivery and drug absorption.[118] Compounds **6v** and **6s** showed high scores (>500), indicating better transdermal delivery. The rest of the synthesized compounds, along with dasatinib, showed moderate or low scores. For the blood-brain barrier, which separates the central nervous system and brain from the bloodstream, a molecule's molecular weight should be less than 480 to be considered a therapeutic agent.[119] The synthesized compounds demonstrated significant results in this regard due to their low molecular weight. The permeability of the Madin-Darby canine kidney (MDCK) cell is often used as a measure of blood-brain barrier permeability, with values greater than 500 indicating a better effect and values less than 25 suggesting a poor outcome, according to Jorgensen's rule of three. Most of the synthesized compounds, as well as dasatinib, exhibited moderate results. Only compounds **6b**, **6c**, **6d**, **6n**, **6o**, **6p**, **6v**, **6w**, and **6x** showed better outcomes. Regarding human oral absorption rate, all of the compounds showed good predictions, except for compounds **6h**, **6u**, **7a**, **7b**, **8a**, and **8b**. In summary, the *in silico* ADME analysis of the synthesized compounds (**6−8**) revealed promising properties for drug development. These compounds exhibited favorable molecular weights, hydrogen bond donor and acceptor values, and octanol/water partition coefficients, comparable to the reference compound Dasatinib. While some compounds showed slightly lower solubility scores, overall, the synthesized compounds demonstrated potential for bioavailability. Notably, compounds **6i** and **6v** exhibited high transdermal delivery scores and demonstrated potency in terms of predicted log IC_{50} values, indicating their potential as effective drugs. Further experimental validation is recommended to confirm these finding.

CONCLUSIONS

In conclusion, this work presents a successful synthetic methodology for the efficient synthesis of dasatinib-like compounds, namely, thiazolyl-indole-2-carboxamide derivatives (**6a-z**, **7a**, **7b**, **8a**, and **8b**). The compounds were evaluated their cytotoxic potential against a broad range of cancer cell lines and a normal cell line. The results demonstrated that compounds **6e**, **6i**, **6q**, **6v**, **7a**, and **7b**, exhibited cytotoxic activity against all tested cancer cell lines. Among them, compounds **6i** and **6v**, containing a dimethyl amine group at the 4-position, exhibited excellent cytotoxic activity against all tested cancer cell lines, especially HeLa and MCF-7, while maintaining lower toxicity toward normal cells (WI-38). All the tested compounds inhibited the enzymatic activities of the target kinases with potencies comparable to reference kinase inhibitors, especially compounds **6i** and **6v** are the most, suggesting their potential as multitargeted kinase inhibitors. Compounds **6i** and **6v** also induced a G2/M phase arrest, potentially impacting cell proliferation and division in MCF-7 cells, and increased apoptosis and necrosis, suggested potential anticancer effects through the promotion of programmed and nonprogrammed cell death. The docking results further demonstrated that the synthesized compounds **6i** and **6v** exhibit improved binding affinity with the target proteins, especially, VEGFR2 kinase and CDK2, respectively, compared to reference drugs dasatinib and others, indicating their potential as kinase inhibitors. Overall, the findings highlight the promising nature of compounds **6i** and **6v** as potential VEGFR2 and CDK2 kinase inhibitors, acting as ATP competitive inhibitors. ADME predictions highlighted the drug-like properties of the synthesized compounds, including favorable pharmacokinetic characteristics. Particularly noteworthy are compounds **6i** and **6v**, which not only demonstrated favorable ADME parameters but also displayed

https://doi.org/10.1021/acsomega.4c06889
ACS Omega 2024, 9, 41944−41967

high transdermal delivery scores and potent predicted log IC_{50} values. Overall, this research provides valuable insights into the synthesis, biological activities, and computational analysis of these compounds, paving the way for their further development as potential anticancer drugs.

EXPERIMENTAL SECTION

General. The chemicals and solvents utilized in this study were of the highest quality available, meeting the standards of commercial reagent grade. The commercially available chemicals (1*H*-indole-2-carboxylic acid, 5-methoxy-1*H*-indole-2-carboxylic acid ethyl 2-(2-aminothiazol-4-yl)acetate, 1,1-carbonyldiimidazole, *N,N′*-Dicyclohexylcarbodiimide (DCC), 1-Ethyl-3-(3-dimethylaminopropyl)carbodiimide (EDC) and substituted benzaldehydes required for the chemical synthesis were procured from AK scientific (Union City, CA, USA). They were procured from reputable suppliers and utilized without any further purification steps. To determine the melting points of the compounds, a Barnstead electrothermal digital melting point apparatus (model IA9100, BIBBY scientific limited, located in Stone, Staffordshire, ST15 0SA, UK) was employed. Infrared (IR) spectra were recorded using a state-of-the-art Jasco FT/IR-6600 spectrometer, manufactured in Japan. Nuclear Magnetic Resonance (NMR) spectra were obtained using a cutting-edge Bruker 700 MHz NMR spectrometry instrument, located in Zurich, Switzerland. An Agilent 6320 ion trap mass spectrometer, equipped with an ESI ion source from Agilent Technologies, Palo Alto, CA, USA, was utilized for mass analysis.

Chemistry. *General Procedure for the Preparation of* ***3****. Synthesis of* Ethyl 2-(2-(1*H*-indole-2-carboxamido)thiazol-4-yl)acetate (**3a**). A mixture of 1*H*-indole-2-carboxylic acid (**1a**, 1.61 g, 0.01 mol) and ethyl-2-(2-aminothiazol-4-yl)acetate (**2**, 1.86 g, 0.01 mol) in CH_2Cl_2 was stirred at 0 °C for 10−15 min. 1-Ethyl-3-(3-dimethylaminopropyl)carbodiimide (EDC, 2.30g, 1.2 equiv) and 4-dimethylaminopyridine (DMAP, 1.22g, 1 equiv) was added to the reaction mixture and was continue stirring for another 5 min at 0 °C. The reaction mixture was then stirred for overnight at room temperature.[23] Formation of solid 1-(3-(dimethylamino)propyl)-3-ethylurea was filtered off. Filtrate was washed with 5% $NaHCO_3$ and water followed by 1 M HCl and Brine. Evaporation of the solvent gave compound **3a**. Orange powder (Yield, 76%). Which was used for the next step without further purification. Mp. 183 °C. FT-IR (KBr), ν (cm^{-1}): 3383, 3300, 2925, 2854, 1720, 1654, 1546, 1371, 1342, 1316, 1288, 1198, 1184, 1021, 876, 825, 742, 725, 650, 547, and 436 cm^{-1}.^{1}H NMR (700 MHz, $CDCl_3$) δ 9.56 (s, 1H), 7.67 (d, J = 8.0 Hz, 1H), 7.44 (d, J = 8.4 Hz, 1H), 7.32 (t, J = 7.7 Hz, 1H), 7.16 (t, J = 7.5 Hz, 1H), 7.13 (s, 1H), 6.85 (s, 1H), 4.17 (q, J = 6.9 Hz, 2H), 3.71 (s, 2H) and 1.24 (t, J = 6.9 Hz, 3H). ^{13}C NMR (176 MHz, $CDCl_3$) δ 170.21, 158.71, 157.88, 143.32, 137.24, 128.38, 127.49, 125.85, 122.66, 121.29, 112.14, 111.27, 105.30, 61.27, 36.97, and 14.18 ppm. Mass (ESI): m/z 330 $[M + H]^+$, 352 $[M + Na]^+$, 368 $[M+K]^+$.

*Ethyl-2-(2-(5-methoxy-1H-indole-2-carboxamido)thiazol-4-yl)acetate (****3b****).* Orange powder (Yield, 87%). Mp. 165 °C. FT-IR (KBr), ν (cm^{-1}): 3291, 3242, 3113, 2985, 2905, 1740, 1645, 1547, 1525, 1453, 1372, 1282, 1214, 1164, 1030, 885, 830, 768, and 736 cm^{-1}. ^{1}H NMR (700 MHz, DMSO-d_6) δ 10.19 (s, 1H), 9.81 (s, 1H), 7.33 (d, J = 9.1 Hz 1H), 7.03 (s, 1H), 7.01 (s, 1H), 6.98 (d, J = 9.4 Hz, 1H), 6.84 (s, 1H), 4.15 (q, J = 6.9 Hz, 2H), 3.82 (s, 3H), 3.70 (s, 2H) and 0.86 (d, t = 8.0 Hz, 3H) ppm. ^{13}C NMR (176 MHz, DMSO-d_6) δ 170.37, 158.92, 157.95, 154.96, 143.62, 132.80, 128.80, 127.86, 117.52, 113.16, 111.28, 104.98, 102.31, 61.22, 55.67, 37.05, and 14.17 ppm. Mass (ESI): m/z 360.06 $[M + H]^+$, 382 $[M + Na]^+$

*1H-indole-2-carbohydrazide (****3c****).* White powder (Yield, 99%). Mp. 125 °C. ^{1}H NMR (700 MHz, DMSO-d_6) δ 11.44 (s, 1H), 9.80 (s, 1H), 7.59 (d, J = 8.0 Hz, 1H), 7.44 (d, J = 8.2 Hz, 1H), 7.18 (t, J = 7.6 Hz, 1H), 7.05 (s, 1H), 7.04 (t, J = 7.4 Hz, 1H) and 4.50 (s, 2H) ppm. ^{13}C NMR (176 MHz, DMSO-d_6) δ 161.79, 136.73, 130.48, 127.47, 123.96, 121.96, 120.44, 112.72, and 102.78 ppm.

*General procedure for the preparation of 4. N-(4-(2-Hydrazineyl-2-oxoethyl)thiazol-2-yl)-1H-indole-2-carboxamide (****4a****).* A suspension of Ethyl 2-(2-(1*H*-indole-2-carboxamido)thiazol-4-yl)acetate (**3**, 1 g, 3.04 mmol) in hydrazine monohydrate (15 mL, 98%) was stirred for 18h at room temperature. To the reaction mixture, water (100 mL) was added and slow evaporation of excess hydrazine using air flow gave colorless precipitate. Precipitate was collected by filtration, washed with excess amount of cold water, dried overnight, yielded compound **4** as off-white solid (82%). Mp. 244 °C. FT-IR (KBr), ν (cm^{-1}): 3379, 3268, 3170, 3054, 1653, 1545, 1412, 1364, 1315, 1285, 1223, 1192, 1145, 990, and 830 cm^{-1}. ^{1}H NMR (700 MHz, DMSO-d_6) δ 12.39 (brs, 1H), 11.86 (s, 1H), 9.15 (s, 1H), 7.65 (d, J = 8.0 Hz, 1H), 7.63 (s, 1H), 7.46 (d, J = 8.2 Hz, 1H), 7.24 (t, J = 7.6 Hz, 1H), 7.07 (t, J = 7.5 Hz, 1H), 6.94 (s, 1H), 4.23 (s, 2H) and 3.46 (s, 2H) ppm. ^{13}C NMR (176 MHz, DMSO-d_6) δ 168.80, 159.65, 158.26, 145.87, 137.76, 129.79, 127.45, 124.92, 122.62, 120.64, 112.94, 110.47, 106.21, and 37.01 ppm. Mass (ESI): m/z 316 $[M + H]^+$, 338 $[M + Na]^+$

*N-(4-(2-hydrazineyl-2-oxoethyl)thiazol-2-yl)-5-methoxy-1H-indole-2-carboxamide (****4b****).* White powder (Yield, 96%). Mp. 218 °C. FT-IR (KBr), ν (cm^{-1}): 3271, 3103, 2830, 1654, 1628, 1550, 1454, 1336, 1280, 1213, 1157, 843, and 730 cm^{-1}. ^{1}H NMR (700 MHz, DMSO-d_6) δ ^{1}H NMR (700 MHz, DMSO) δ 12.63 (s, 1H), 11.74 (s, 1H), 9.17 (s, 1H), 7.58 (s, 1H), 7.37 (d, J = 8.8 Hz, 1H), 7.13 (d, J = 2.7 Hz, 1H), 6.95 (s, 1H), 6.92 (dd, J = 8.8, 2.6 Hz, 1H), 4.27 (s, 2H), 3.78 (s, 3H) and 3.48 (s, 2H) ppm. ^{13}C NMR (176 MHz, DMSO-d_6) δ 168.81, 159.54, 158.23, 154.44, 145.86, 133.14, 129.93, 127.76, 116.55, 113.82, 110.45, 105.91, 102.57, 55.73, and 37.01 ppm. Mass (ESI): m/z 346 $[M + H]^+$, 368 $[M + Na]^+$.

General procedure for the preparation of ***6a−6z****.* A mixture of *N*-(4-(2-Hydrazineyl-2-oxoethyl)thiazol-2-yl)-1*H*-indole-2-carboxamide (**4a**, 100 mg, 0.317 mmol) was mixed with an equivalent amount of substituted-aldehyde (**5**, 1 equiv) and dissolved in 10 mL of absolute ethanol. A catalytic amount of glacial acetic acid (3−4 drops) was added to the reaction mixture, which was then refluxed for 18 h. The resulting precipitate was filtered, washed with cold ethanol, and dried under vacuum to yield the desired product

*(E/Z)-N-(4-(2-(2-Benzylidenehydrazineyl)-2-oxoethyl)-thiazol-2-yl)-1H-indole-2-carboxamide (****6a****).* Colorless powder (Yield, 95%). Mp. 217 °C. FT-IR (KBr), ν (cm^{-1}): 3437, 3371, 3196, 3083, 2983, 1682, 1655, 1539, 1419, 1316, 1275, 1227, 1203, 1184, 1144, 950, 790, 757, 741, 689, 574, 543, 507, and 487 cm^{-1}. ^{1}H NMR (700 MHz, DMSO-d_6) δ 12.69 (s, 1.7H), 11.87 (s, 0.7H), 11.86 (s, 1H), 11.57 (s, 0.7H), 11.45 (s, 1H), 8.22 (s, 0.7H), 8.00 (s, 1H), 7.72−7.61 (m, 6.8H), 7.48−7.36 (m, 6.8H), 7.24 (t, J = 7.6 Hz, 1.7H), 7.06 (t, J = 7.5 Hz, 1.7H), 7.03 (s, 0.7H), 7.01 (s, 1H), 4.09 (s, 2H) and 3.65 (s, 1.4H). ^{13}C NMR (176 MHz, DMSO-d_6) δ 171.64, 165.88, 159.61, 159.55, 158.33, 158.01, 146.92, 145.64, 145.45,

https://doi.org/10.1021/acsomega.4c06889
ACS Omega 2024, 9, 41944−41967

143.32, 137.78, 137.76, 134.74, 134.71, 130.49, 130.24, 129.70, 129.31, 129.29, 127.51, 127.45, 127.22, 124.96, 124.93, 122.63, 120.64, 112.94, 110.95, 110.75, 106.28, 106.20, 37.91, and 35.53 ppm. Mass (ESI): m/z 404 $[M + H]^+$, 426 $[M + Na]^+$. Purity 95.3% (R_t = 18.9 min).

*(E/Z)-N-(4-(2-(2-(4-Bromobenzylidene)hydrazineyl)-2-oxoethyl)thiazol-2-yl)-1H-indole-2-carboxamide (**6b**).* White powder (Yield, 97%). Mp. 261 °C. FT-IR (KBr), ν (cm^{-1}): 3437, 3320, 3219, 3148, 2911, 1633, 1548, 1382, 1342, 1318, 1275, 1227, 1179, 1131, 955, 822, 741, 576, 511, and 434 cm^{-1}. ^1H NMR (700 MHz, DMSO-d_6) δ 12.70 (s, 1.7H), 11.89 (s, 0.7H), 11.88 (s, 1H), 11.66 (s, 0.7H), 11.54 (s, 1H), 8.21 (s, 0.7H), 7.99 (s, 1H), 7.66 (t, overlapped, J = 7 Hz, 7H), 7.48 (d, J = 8.7 Hz, 1.7H), 7.30−7.24 (m, 1.7H), 7.08 (t, J = 7.7 Hz, 1.7H), 7.05 (s, 0.7H), 7.03 (s, 1H), 4.10 (s, 2H) and 3.68 (s, 1.4H) ppm. ^{13}C NMR (176 MHz, DMSO-d_6) δ ^{13}C NMR (176 MHz, DMSO DMSO-d_6) δ 171.72, 159.56, 158.33, 158.02, 145.70, 145.56, 145.37, 142.13, 137.77, 134.01, 132.30, 129.69, 129.38, 129.12, 127.45, 124.95, 123.70, 123.40, 122.63, 120.65, 112.94, 110.98, 110.79, 106.22, 37.89, and 35.52 ppm. Mass (ESI): m/z 482 $[^{79}(Br)M+H]^+$, 484 $[^{81}(Br)M+H]^+$; 504 $[^{79}(Br)M+Na]^+$, 506 $[^{81}(Br)M+Na]^+$, 522 $[^{81}(Br)M+K]^+$. Purity 98.7% (R_t = 17.63 min).

*(E/Z)-N-(4-(2-(2-(4-Chlorobenzylidene)hydrazineyl)-2-oxoethyl)thiazol-2-yl)-1H-indole-2-carboxamide (**6c**).* White powder (Yield, 98%). Mp. 236 °C. FT-IR (KBr), ν (cm^{-1}): 3440, 3321, 3214, 1670, 1634, 1550, 1382, 1319, 1260, 1225, 1092, 1021, 797, 741, 649, 514, and 460 cm^{-1}. ^1H NMR (700 MHz, DMSO-d_6) δ 12.68 (s, 1.7H), 11.87 (s, 0.7H), 11.86 (s, 1H), 11.63 (s, 0.7H), 11.51 (s, 1H), 8.21 (s, 0.7H), 7.98 (s, 1H), 7.72 (d, overlapped, 1.4H), 7.72 (d, overlapped, J = 7.0 Hz, 2H), 7.66 (d, overlapped, 1.4H), 7.64 (d, overlapped, 1.4H), 7.51 (d, overlapped, 1.4H), 7.49 (d, overlapped, J = 7.0 Hz, 2H), 7.46 (s, 0.7H), 7.45 (s, 1H), 7.49 (t, J = 7.0 Hz, 1.7H), 7.06 (t, J = 7.0 Hz, 1.7H), 7.03 (s, 0.7H), 7.01 (s, 1H), 4.08 (s, 2H) and 3.66 (s, 1.4H) ppm. ^{13}C NMR (176 MHz, DMSO) δ 171.72, 165.97, 159.61, 159.55, 158.33, 158.02, 145.61, 145.57, 145.38, 142.02, 137.78, 137.76, 134.90, 134.63, 133.71, 133.67, 129.69, 129.65, 129.39, 129.15, 128.88, 127.44, 127.43, 124.96, 124.94, 122.63, 120.65, 112.94, 110.97, 110.78, 106.29, 106.21, 37.89, and 35.52 ppm. Mass (ESI): m/z 438 $[^{35}(Cl)M+H]^+$, 440 $[^{37}(Cl)M+H]^+$, 460 $[^{35}(Cl)M + Na]^+$, 462 $[^{37}(Cl)M+Na]^+$. Purity 97.9% (R_t = 25.79 min).

*(E/Z)-N-(4-(2-(2-(4-Fluorobenzylidene)hydrazineyl)-2-oxoethyl)thiazol-2-yl)-1H-indole-2-carboxamide (**6d**).* White powder (Yield, 97%). Mp. 262 °C. FT-IR (KBr), ν (cm^{-1}): 3421, 3229, 3083, 1669, 1646, 1604, 1558, 1540, 1508, 1418, 1232, 1232, 1152, 932, 835, and 746 cm^{-1}. ^1H NMR (700 MHz, DMSO-d_6) δ 12.70 (s, 1.7H), 11.89 (s, 0.7H), 11.88 (s, 1H), 11.60 (s, 0.7H), 11.48 (s, 1H), 8.24 (s, 0.7H), 8.01 (s, 1H), 7.76 (q, J = 9.4, 6.2 Hz, 3.5H), 7.67 (d, J = 12.5 Hz, 3.5H), 7.48 (d, J = 8.4 Hz, 1.7H), 7.28 (dq, J = 15.2, 8.2, 7.4 Hz, 5.25H), 7.09 (t, J = 7.7 Hz, 1.7H), 7.05 (s, 0.7H), 7.03 (s, 1H), 4.10 (s, 2H) and 3.67 (s, 1.4H) ppm. ^{13}C NMR (176 MHz, DMSO-d_6) δ 171.68, 165.98, 164.63, 164.08, 162.85, 162.67, 159.61, 159.56, 145.88, 145.62, 145.41, 142.25, 137.77, 137.76, 131.31, 129.73, 129.68, 129.63, 129.40, 129.35, 127.44, 125.00, 124.97, 122.63, 120.68, 116.42, 116.29, 112.95, 110.98, 110.76, 106.30, 106.22, 37.85, and 35.53 ppm. Mass (ESI): m/z 422 $[M + H]^+$; 444 $[M + Na]^+$. Purity 98.7% (R_t = 28.63 min).

*(E/Z)-N-(4-(2-(2-(4-Hidroxybenzylidene)hydrazineyl)-2-oxoethyl)thiazol-2-yl)-1H-indole-2-carboxamide (**6e**).* White powder (Yield, 97%). Mp. 304 °C. FT-IR (KBr), ν (cm^{-1}): 3382, 3348, 3145, 3087, 2989, 2941, 1655, 1613, 1604, 1432, 1392, 1341, 1315, 1275, 1232, 1190, 1165, 1117, 857, 830, 743, 732, 642, 532, and 426 cm^{-1}. ^1H NMR (700 MHz, DMSO-d_6) δ 12.70 (s, 1.8H), 11.89 (s, 0.8H), 11.88 (s, 1H), 11.38 (s, 0.8H), 11.26 (s, 1H), 9.91 (s, 0.8H), 9.87 (s, 1H), 8.12 (s, 0.8H), 7.91 (s, 1H), overlapped (m, 3.6H), 7.53 (d, J = 8.1 Hz, 1.6H), 7.51 (d, J = 8.3 Hz, 2H), 7.48 (s, 1H), 7.47 (s, 1H), 7.26 (t, J = 7.6 Hz, 1.8H), 7.09 (t, J = 7.5 Hz, 1.8H), 7.04 (s, 0.8H), 7.01 (s, 1H), 6.82 (overlapped, 3.6H), 4.07 (s, 2H) and 3.64 (s, 1.6H) ppm. ^{13}C NMR (176 MHz, DMSO-d_6) δ 171.27, 165.49, 159.82, 159.58, 159.53, 158.27, 157.95, 147.20, 145.79, 145.64, 143.60, 137.77, 137.76, 129.71, 129.66, 129.25, 128.91, 127.44, 125.72, 125.69, 124.96, 124.93, 122.63, 120.65, 116.16, 116.14, 112.94, 110.83, 110.68, 106.27, 106.19, 37.90, and 35.45 ppm. Mass (ESI): m/z 420 $[M + H]^+$, 442 $[M + Na]^+$, 458 $[M+K]^+$. Purity 96.4% (R_t = 13.51 min).

*(E/Z)-N-(4-(2-(2-(2-Methoxybenzylidene)hydrazineyl)-2-oxoethyl)thiazol-2-yl)-1H-indole-2-carboxamide (**6f**).* Yellow powder (Yield, 96%). Mp. 230 °C. FT-IR (KBr), ν (cm^{-1}): 3212, 3135, 2992, 2839, 1893, 1674, 1642, 1611, 1564, 1377, 1343, 1316, 1288, 1249, 1203, 1145, 827, 743, and 458 cm^{-1}. ^1H NMR (700 MHz, DMSO-d_6) δ 12.70 (s, 1H), 11.99 (s, 0.75H), 11.89 (s, 0.75H), 11.88 (s, 1H), 11.59 (s, 0.75H), 11.43 (s, 1H), 8.58 (s, 0.75H), 8.36 (s, 1H), 7.82 (t, J = 9.0 Hz, 1.75H), 7.66 (dd, J = 10.6, 6.4 Hz, 3.5H), 7.48 (d, J = 8.4 Hz, 1.75H), 7.41 (dt, J = 14.3, 7.9 Hz, 1.75H), 7.26 (t, J = 7.7 Hz, 1.75H), 7.10 (dt, J = 14.0, 8.2 Hz, 3.5H), 7.05 (s, 0.75H), 7.01 (s, 2.75H), 4.09 (s, 2H), 3.86 (d, J = 12.6 Hz, 5.25H) and 3.65 (s, 1.5H) ppm. ^{13}C NMR (176 MHz, DMSO-d_6) δ 172.49, 171.52, 165.68, 159.63, 159.61, 158.34, 158.32, 158.14, 158.01, 142.39, 138.94, 137.78, 137.76, 131.98, 131.69, 129.75, 129.70, 127.45, 127.44, 125.91, 125.75, 124.96, 124.92, 122.71, 122.65, 122.62, 121.23, 120.65, 120.64, 112.94, 112.29, 112.27, 110.93, 110.66, 106.26, 106.18, 56.18, 56.14, 37.91, and 35.53 ppm. Mass (ESI): m/z 434 $[M + H]^+$; 456 $[M + Na]^+$. Purity 96.1% (R_t = 19.22 min).

*(E/Z)-N-(4-(2-(2-(4-Methoxybenzylidene)hydrazineyl)-2-oxoethyl)thiazol-2-yl)-1H-indole-2-carboxamide (**6g**).* Yellowish powder (Yield, 98%). Mp. 253 °C. FT-IR (KBr), ν (cm^{-1}): 3413, 3227, 3055, 2845, 1651, 1542, 1480, 1386, 1313, 1249, 1176, 1130, 1029, 926, 846, 739, 724, 642, 618, 524, and 432 cm^{-1}. ^1H NMR (700 MHz, DMSO-d_6) δ 12.68 (s, 1.8H), 11.87 (s, 0.8H), 11.86 (s, 1H), 11.43 (s, 0.8H), 11.32 (s, 1H), 8.15 (s, 0.8H), 7.94 (s, 1H), 7.63 (dq, J = 15.6, 8.7 Hz, 7.2H), 7.46 (s, 1H), 7.45 (s, 0.8H), 7.24 (t, J = 7.7 Hz, 1.8H), 7.06 (t, J = 7.5 Hz, 1.8H), 7.02 (s, 0.8H), 6.99 (dt, J = 10.3, 6.0 Hz, 4.6H), 4.06 (s, 2H), 3.79 (s, 2.3H), 3.78 (s, 3H) and 3.63 (s, 1.6H) ppm. ^{13}C NMR (176 MHz, DMSO-d_6) δ 13C NMR (176 MHz, DMSO) δ 171.39, 165.62, 161.25, 161.03, 159.60, 159.54, 158.29, 157.97, 146.79, 145.75, 145.58, 143.18, 137.76, 129.70, 129.66, 129.10, 128.78, 127.44, 127.30, 127.28, 124.95, 122.63, 120.65, 114.79, 112.94, 110.86, 110.69, 106.27, 106.19, 55.77, 55.75, 37.90, and 35.50 ppm. Mass (ESI): m/z 434 $[M + H]^+$. Purity 97.7% (R_t = 20.44 min).

*(E/Z)-N-(4-(2-(2-(4-Nitrobenzylidene)hydrazineyl)-2-oxoethyl)thiazol-2-yl)-1H-indole-2-carboxamide (**6h**).* Yellow powder (Yield, 99%). Mp. 256 °C. FT-IR (KBr), ν (cm^{-1}): 3424, 3397, 3217, 3144, 2359, 1673, 1634, 1561, 1518, 1402, 1340, 1313, 1194, 1146, 1070, 838, 747, 687, 550, and 434 cm^{-1}. ^1H NMR (700 MHz, DMSO-d_6) δ 12.71 (s, 1.6H), 11.91 (s, 0.6H), 11.89 (s, 0.6H), 11.88 (s, 1H), 11.78 (s, 1H), 8.35 (s, 0.6H), 8.31 (d, J = 8.2 Hz, 1.2H), 8.29 (d, J =

https://doi.org/10.1021/acsomega.4c06889
ACS Omega 2024, 9, 41944−41967

8.8 Hz, 2H), 8.12 (s, 1H), 7.98 (d, J = 8.8 Hz, 1.2H), 7.97 (d, J = 8.8 Hz, 2H) 7.67 (d, J = 8.6 Hz, 3.2H), 7.48 (s, 0.6H), 7.48 (s, 1H), 7.27 (d, J = 7.6 Hz, 0.6H), 7.26 (d, J = 7.6 Hz, 16H), 7.09 (d, J = 7.5 Hz, 1.2H), 7.07 (d, J = 7.5 Hz, 2H), 4.14 (s, 2H) and 3.72 (s, 1.2H) ppm. ^{13}C NMR (176 MHz, DMSO) δ 172.06, 166.35, 159.57, 158.39, 158.09, 148.30, 148.10, 145.39, 145.18, 144.51, 141.12, 141.04, 140.99, 137.77, 129.67, 128.45, 128.17, 127.44, 124.96, 124.54, 122.63, 120.65, 112.94, 111.09, 110.90, 106.30, 106.23, 37.90, and 35.63 ppm. Mass (ESI): m/z 449 $[M + H]^+$, 471 $[M + Na]^+$, 487 $[M+K]^+$. Purity 96.6% (R_t = 16.66 min).

(E/Z)-N-(4-(2-(2-(4-(Dimethylamino)benzylidene)-hydrazineyl)-2-oxoethyl)thiazol-2-yl)-1H-indole-2-carboxamide ***(6i)***. Orange powder (Yield, 96%). Mp. 269 °C. FT-IR (KBr), ν (cm^{-1}): 3414, 3217, 3140, 2891, 2810, 1666, 1607, 1537, 1365, 1314, 1182, 949, 742, and 520 cm^{-1}. ^{1}H NMR (700 MHz, DMSO-d_6) δ 12.67 (s, 1.8H), 11.87 (s, 0.8H), 11.86 (s, 1H), 11.26 (s, 0.8H), 11.16 (s, 1.0H), 8.06 (s, 0.8H), 7.86 (s, 1H), 7.65 (s, 0.8H), 7.64 (s, 3H), 7.53−7.42 (m, 5.6H), 7.24 (t, J = 7.7 Hz, 1.8H), 7.06 (t, J = 7.7 Hz, 1.8H), 7.01 (s, 0.8H), 6.98 (s, 1H), 6.72 (t, J = 8.1 Hz, 3.6H), 4.04 (s, 2H), 3.61 (s, 1.6H), 2.95 (s, 6H) and 2.94 (s, 4.8H) ppm. ^{13}C NMR (176 MHz, DMSO) δ 172.49, 171.03, 165.25, 159.62, 158.31, 158.01, 151.94, 151.75, 147.69, 145.70, 144.12, 137.78, 137.76, 129.77, 129.71, 128.81, 128.47, 127.46, 127.44, 124.95, 124.92, 122.63, 122.61, 122.11, 121.99, 120.65, 120.64, 112.94, 112.31, 112.27, 110.75, 110.59, 106.25, 106.17, 37.91, 35.44, and 21.54 ppm. Mass (ESI): m/z 447 $[M + H]^+$. Purity 95.5% (R_t = 19.78 min).

(E/Z)-N-(4-(2-(2-(4-(Methylthio)benzylidene)hydrazineyl)-2-oxoethyl)thiazol-2-yl)-1H-indole-2-carboxamide ***(6j)***. White powder (Yield, 96%). Mp. 196 °C. FT-IR (KBr), ν (cm^{-1}): 3350, 3317, 3250, 3074, 2911, 1674, 1661, 1595, 1540, 1494, 1343, 1315, 1290, 1230, 1211, 1190, 1143, 1092, 1072, 961, 871, 813, 742, 731, 565, and 431 cm^{-1}. ^{1}H NMR (700 MHz, DMSO-d_6) δ 12.70 (s, 1.75H), 11.89 (s, 0.75H), 11.88 (s, 1H), 11.54 (s, 0.75H), 11.43 (s, 1H), 8.18 (s, 0.75H), 7.97 (s, 1H), 7.68 (s, 0.75H), 7.66 (s, 2.75H), 7.64 (d, J = 7.6 Hz, 1.50H), 7.62 (d, J = 8.2 Hz, 2H), 7.48 (d, J = 8.6 Hz, 1.75H), 7.32 (t, J = 9.6 Hz, 3.5H), 7.26 (t, J = 7.7 Hz, 1.75H), 7.09 (t, J = 7.5 Hz, 1.75H), 7.05 (s, 0.75H), 7.02 (s, 1H), 4.09 (s, 2H), 3.66 (s, 1.50H) and 2.52 (s, 5.25H) ppm. ^{13}C NMR (176 MHz, DMSO-d_6) δ 171.52, 165.76, 159.54, 157.99, 146.51, 145.66, 145.49, 142.93, 141.35, 140.99, 1.37.77, 137.76, 131.17, 131.16, 129.69, 129.65, 127.92, 127.64, 127.45, 126.16, 126.11, 124.96, 124.94, 122.63, 120.65, 112.94, 110.91, 110.73, 106.28, 106.20, 37.91, 35.52, 14.75, and 14.72 ppm. Mass (ESI): m/z 450 $[M + H]^+$; 472 $[M + Na]^+$; 488 $[M+K]^+$. Purity 97.7% (R_t = 28.95 min).

(E/Z)-N-(4-(2-(2-(2-Hydroxy-4-methoxybenzylidene)-hydrazineyl)-2-oxoethyl)thiazol-2-yl)-1H-indole-2-carboxamide ***(6k)***. Yellow powder (Yield, 97%). Mp. 244 °C. FT-IR (KBr), ν (cm^{-1}): 3213, 3154, 2836, 1669, 1631, 1537, 1400, 1342, 1312, 1282, 1223, 1187, 1163, 963, 871, 740, 572, 468, and 430 cm^{-1}. ^{1}H NMR (700 MHz, DMSO-d_6) δ 12.70 (s, 1.4H), 11.89 (s, 1H), 11.88 (s, 0.4H), 11.71 (s, 1H), 11.47 (s, 1H), 11.31 (s, 0.4H), 10.22 (s, 0.4H), 8.34 (s, 1H), 8.21 (s, 0.4H), 7.68 (s, 0.8H), 7.67 (s, 2H), 7.57 (s, 0.4H), 7.48 (d, J = 8.4 Hz, 1.4H), 7.42 (d, J = 8.6 Hz, 1H), 7.26 (t, J = 7.7 Hz, 1.4H), 7.09 (t, J = 7.6 Hz, 1.4H), 7.06 (s, 1H), 7.00 (s, 0.4H), 6.52 (d, J = 8.6 Hz, 1H), 6.49 (d, J = 6.2 Hz, 0.4H), 6.49 (s, 1H), 6.45 (s, 0.4H), 4.03 (s, 0.8H), 3.77 (s, 3H), 3.75 (s, 1.2H) and 3.67 (s, 2H) ppm. ^{13}C NMR (176 MHz, DMSO-d_6) δ 170.86, 165.45, 162.48, 162.20, 159.73, 159.61, 158.36, 147.98, 145.28, 141.96, 137.78, 137.76, 131.50, 129.65, 128.69, 127.43, 124.97, 124.93, 122.64, 122.62, 120.65, 120.64, 113.47, 112.94, 112.14, 111.06, 106.91, 106.89, 106.28, 106.20, 101.60, 101.40, 55.78, 55.65, 37.62, and 35.63 ppm. Mass (ESI): m/z 450 $[M + H]^+$, 472 $[M + Na]^+$. Purity 95.3% (R_t = 23.49 min).

(E/Z)-N-(4-(2-(2-(Naphthalen-1-ylmethylene)hydrazineyl)-2-oxoethyl)thiazol-2-yl)-1H-indole-2-carboxamide ***(6l)***. White powder (Yield, 96%). Mp. 269 °C. FT-IR (KBr), ν (cm^{-1}): 3420, 3227, 3054, 1676, 1540, 1395, 1340, 1313, 1286, 1185, 1144, 768, and 743 cm^{-1}. ^{1}H NMR (700 MHz, DMSO-d_6) δ 12.72 (s, 1.75H), 11.90 (s, 0.75H), 11.88 (s, 1H), 11.69 (s, 0.75H), 11.53 (s, 1H), 8.86 (overlapped, J = 4.3 Hz, 1.75H), 8.70 (s, 1H), 8.63 (d, J = 8.6 Hz, 1H), 8.02 (t, J = 6.5 Hz, 3.5H), 7.90 (d, J = 7.4 Hz, 1.75H), 7.67 (d, J = 8.2 Hz, 5.25H), 7.61 (q, overlapped, J = 10.3, 9.0 Hz, 3.5H), 7.48 (d, J = 8.5 Hz, 1.75H), 7.26 (t, J = 7.6 Hz, 1.75H), 7.13−7.04 (d, overlapped, 3.5H), 4.18 (s, 2H) and 3.74 (s, 1H) ppm. ^{13}C NMR (176 MHz, DMSO-d_6) δ 171.98, 166.48, 159.69, 158.20. 147.15, 145.40, 143.90, 137.72, 137.70, 133.92, 131.18, 130.90, 130.53, 130.36, 129.71, 129.65, 129.49, 129.27, 128.38, 128.11, 127.90, 127.85, 127.38, 126.87, 126.83, 126.07, 125.23, 125.20, 124.54, 124.36, 122.68, 120.87, 120.85, 112.94, 111.24, 110.76, 106.39, 106.35, 37.73, and 35.89 ppm. Mass (ESI): m/z 454$[M + H]^+$; 476 $[M + Na]^+$; 493 $[M+K]^+$. Purity 98.9% (R_t = 18.46 min).

(E/Z)-N-(4-(2-(2-Benzylidenehydrazineyl)-2-oxoethyl)-thiazol-2-yl)-5-methoxy-1H-indole-2-carboxamide ***(6m)***. White powder (Yield, 97%). Mp. 239 °C. FT-IR (KBr), ν (cm^{-1}): 3222, 3141, 3077, 2833, 1678, 1649, 1556, 1523, 1412, 1284, 1213, 1161, 885, 832, 748, 687, and 540 cm^{-1}. ^{1}H NMR (700 MHz, DMSO-d_6) δ 12.62 (s, 1H), 11.95 (s, 0.7H), 11.73 (s, 0.7H), 11.71 (s, 1H), 11.57 (s, 0.7H), 11.45 (s, 1H), 8.22 (s, 0.7H), 8.00 (s, 1H), 7.69 (d, J = 7.3 Hz, 1.4H), 7.67 (d, J = 7.4 Hz, 2H), 7.55 (s, 1.7H), 7.42 (m, 5.1H), 7.34 (d, J = 9.0 Hz, 1.7H), 7.10 (s, 1.7H), 7.02 (s, 0.7H), 7.00 (s, 1H), 6.89 (d, J = 9.1 Hz, 1.7H), 4.08 (s, 2H), 3.76 (s, 3H), 3.76, (s, 2.1H) and 3.65 (s, 1.4H) ppm. ^{13}C NMR (176 MHz, DMSO-d_6) δ 172.49, 171.64, 165.89, 154.44, 146.92, 143.32, 134.74, 134.71, 133.16, 133.14, 130.49, 130.24, 129.32, 129.29, 127.76, 127.51, 127.22, 116.58, 116.54, 113.81, 110.67, 105.95, 105.87, 102.57, 55.73, 37.89, and 35.50 ppm. Mass (ESI): m/z 434 $[M + H]^+$, 456 $[M + Na]^+$. Purity 98.7% (R_t = 15.77 min).

(E/Z)-N-(4-(2-(2-(4-Bromobenzylidene)hydrazineyl)-2-oxoethyl)thiazol-2-yl)-5-methoxy-1H-indole-2-carboxamide ***(6n)***. Yellow powder (Yield, 97%). Mp. 280 °C. FT-IR (KBr), ν (cm^{-1}): 3450, 3307, 3206, 2988, 1671, 1637, 1542, 1483, 1454, 1381, 1325, 1278, 1228, 1178, 1134, 1066, 1027, 1008, 953, 876, 852, 814, 757, 713, 571, 511, and 433 cm^{-1}. ^{1}H NMR (700 MHz, DMSO-d_6) δ 12.62 (s, 1.7H), 11.73 (s, 0.7H), 11.72 (s, 1H), 11.64 (s, 0.7H), 11.51 (s, 1H), 8.19 (s, 0.7H), 7.97 (s, 1H), 7.64 (ABq, J = 8.0, 1.1 Hz, 2.8H), 7.62 (ABq, J = 8.1, 0.9 Hz, 4H), 7.56 (s, 1.7H), 7.35 (d, J = 8.8 Hz, 1.7H), 7.10 (d, J = 2.6 Hz, 1.7H), 7.02 (s, 0.7H), 7.00 (s, 1H), 6.89 (ddd, J = 8.9, 2.5, 1.1 Hz, 1.7H), 4.07 (s, 2H), 3.76 (s, 3H), 3.75 (s, 2.1H) and 3.65 (s, 1.4H) ppm. ^{13}C NMR (176 MHz, DMSO-d_6) δ 171.73, 165.99, 159.52, 159.47, 158.38, 158.07, 154.44, 145.69, 145.53, 145.34, 142.12, 134.05, 134.01, 133.16, 133.14, 132.30, 129.88, 129.84, 129.38, 129.11, 127.76, 123.70, 123.40, 116.59, 116.56, 113.82, 110.92, 110.73, 105.97, 105.89, 102.57, 55.73, 37.89, and 35.51 ppm. Mass (ESI): m/z 512 $[^{79}(Br)M+H]^+$, 514 $[^{81}(Br)M+H]^+$, 534 $[^{79}(Br)M+Na]^+$, 536 $[^{81}(Br)M+Na]^+$. Purity 97.4% (R_t = 17.43 min).

https://doi.org/10.1021/acsomega.4c06889
ACS Omega 2024, 9, 41944−41967

*(E/Z)-N-(4-(2-(2-(4-Chlorobenzylidene)hydrazineyl)-2-oxoethyl)thiazol-2-yl)-5-methoxy-1H-indole-2-carboxamide (**6o**)*. White powder (Yield, 96%). Mp. 261 °C. FT-IR (KBr), ν (cm^{-1}): 3205, 3060, 2943, 2825, 1676, 1649, 1542, 1488, 1454, 1398, 1340, 1278, 1213, 1157, 1090, 1012, 985, 849, 825, 731, and 514 cm^{-1}. ^{1}H NMR (700 MHz, DMSO-d_6) δ 12.62 (s, 1.7H), 11.73 (s, 0.7H), 11.71 (s, 1H), 11.63 (s, 0.7H), 11.51 (s, 1H), 8.21 (s, 0.7H), 7.99 (s, 1H), 7.73−7.68 (overlapped, 3.4H), 7.55 (s, 1.7H), 7.51−7.46 (overlapped, 3.4H), 7.34 (d, J = 9.0 Hz, 1.7H), 7.10 (s, 1.7H), 7.02 (s, 0.7H), 7.00 (s, 1H), 6.89 (d, J = 8.9 Hz, 1.7H), 4.08 (s, 2H), 3.76 (s, 5.1H) and 3.65 (s, 1.4H) ppm. ^{13}C NMR (176 MHz, DMSO-d_6) δ 171.72, 165.98, 159.51, 158.39, 158.19, 154.44, 145.61, 142.03, 134.91, 134.63, 133.72, 133.67, 133.14, 131.61, 129.85, 129.39, 129.15, 128.88, 127.76, 116.58, 116.55, 113.82, 110.91, 110.71, 105.97, 105.89, 102.57, 55.73, 37.88, and 35.51 ppm. Mass (ESI): m/z 468 [^{35}(Cl)M+H]$^+$, 470 [^{37}(Br)M +H]$^+$, 490 [^{35}(Cl)M+Na]$^+$, 492 [^{37}(Cl)M+Na]$^+$. Purity 97.5% (R_t = 29.00 min).

*(E/Z)-N-(4-(2-(2-(4-Fluorobenzylidene)hydrazineyl)-2-oxoethyl)thiazol-2-yl)-5-methoxy-1H-indole-2-carboxamide (**6p**)*. White powder (Yield, 98%). Mp. 180 °C. FT-IR (KBr), ν (cm^{-1}): 3364, 3204, 3050, 2940, 2829, 1678, 1650, 1542, 1508, 1453, 1339, 1278, 1231, 1212, 115, 1120, 835, 730, and 524 cm^{-1}. ^{1}H NMR (700 MHz, DMSO-d_6) δ 12.62 (s, 1.7H), 11.73 (s, 0.7H), 11.72 (s, 1H), 11.57 (s, 0.7H), 11.46 (s, 1H), 8.22 (s, 0.7H), 7.99 (s, 1H), 7.74 (dt, J = 12.6, 6.6 Hz, 3.4H), 7.56 (s, 1.7H), 7.34 (d, J = 8.9 Hz, 1.7H), 7.27 (q, J = 9.2 Hz, 3.4H), 7.10 (s, 1.7H), 7.02 (s, 0.7H), 6.99 (s, 1H), 6.89 (d, J = 8.9 Hz, 1.7H), 4.07 (s, 2H), 3.76 (s, 5.1H) and 3.65 (s, 1.4H) ppm. ^{13}C NMR (176 MHz, DMSO-d_6) δ ^{13}C NMR (176 MHz, DMSO) δ 171.65, 165.90, 164.25, 164.07, 162.85, 162.67, 159.54, 158.39, 158.08, 154.44, 145.81, 145.59, 145.40, 142.17, 133.16, 133.14, 131.36, 131.33, 129.92, 129.88, 129.70, 129.65, 129.40, 129.35, 127.76, 116.58, 116.55, 116.42, 116.29, 113.82, 110.88, 110.67, 105.96, 105.88, 102.57, 55.73, 37.88, and 35.52 ppm. Mass (ESI): m/z 452 [M + H]$^+$, 474 [M + Na]$^+$. Purity 99.5% (R_t = 24.60 min).

*(E/Z)-N-(4-(2-(2-(4-Hydroxybenzylidene)hydrazineyl)-2-oxoethyl)thiazol-2-yl)-5-methoxy-1H-indole-2-carboxamide (**6q**)*. Colorless powder (Yield, 95%). Mp. 275 °C. FT-IR (KBr), ν (cm^{-1}): 3414, 3354, 3220, 2933, 2829, 1661, 1606, 1552, 1514, 1454, 1343, 1280, 1214, 1165, 1031, 835, 751, 729, and 530 cm^{-1}. ^{1}H NMR (700 MHz, DMSO-d_6) δ 12.61 (s, 1.8H), 11.73 (s, 0.8H), 11.71 (s, 1H), 11.35 (s, 0.8H), 11.24 (s, 1H), 9.89 (s, 0.8H), 9.86 (s, 1H), 8.10 (s, 0.8H), 7.89 (s, 1H), 7.55 (s, 1.8H), 7.51 (dd, J = 8.3, 2.3 Hz, 1.6H), 7.49 (dd, J = 8.3, 2.3 Hz, 2H), 7.34 (d, J = 8.9 Hz, 1.8H), 7.10 (s, 2H), 7.00 (s, 0.8H), 6.98 (s, 1H), 6.89 (d, J = 8.9 Hz, 1.8H), 6.80 (t, J = 6.6 Hz, 3.6H), 4.04 (s, 2H), 3.76 (s, 5.4H) and 3.61 (s, 1.6H) ppm. ^{13}C NMR (176 MHz, DMSO-d_6) δ 171.28, 165.50, 159.83, 159.59, 159.55, 158.33, 158.07, 154.45, 147.20, 145.67, 143.61, 133.16, 133.14, 129.95, 129.90, 129.26, 128.92, 127.77, 125.73, 125.70, 116.58, 116.54, 116.17, 116.15, 113.82, 110.77, 110.61, 105.95, 105.87, 102.58, 55.73, 37.89, and 35.43 ppm. Mass (ESI): m/z 450 [M + H]$^+$, 488 [M+K]$^+$. Purity 98.3% (R_t = 20.52 min).

*(E/Z)-5-Methoxy-N-(4-(2-(2-(4-methylbenzylidene)-hydrazineyl)-2-oxoethyl)thiazol-2-yl)-1H-indole-2-carboxamide (**6r**)*. White powder (Yield, 97%). Mp. 228 °C. FT-IR (KBr), ν (cm^{-1}): 3219, 3165, 3141, 1678, 1650, 1554, 1524, 1454, 1413, 1284, 1254, 1213, 1161, 1116, 1033, 928, 884, 837, 801, 752, 714, 626, 512, 458, and 430 cm^{-1}. ^{1}H NMR (700 MHz, DMSO-d_6) δ ^{1}H NMR (700 MHz, DMSO) δ 12.64 (s, 1H), 11.97 (s, 0.7H), 11.75 (s, 0.7H), 11.74 (s, 1H), 11.57 (s, 0.7H), 11.40 (s, 1H), 8.50 (s, 0.7H), 8.30 (s, 1H), 7.79 (d, J = 8.0 Hz, 0.7H), 7.75 (d, J = 7.7 Hz, 1H), 7.58 (dd, J = 4.4, 2.3 Hz, 1.7H), 7.37 (d, J = 9.0 Hz, 1.7H), 7.31 (ddd, J = 9.0, 7.3, 2.7 Hz, 1.7H), 7.26 (q, J = 6.3, 5.1 Hz, 3.4H), 7.13 (s, 0.7H), 7.12 (s, 1H), 7.05 (s, 0.7H), 7.01 (s, 1H), 6.92 (dt, J = 8.9, 2.0 Hz, 1.7H), 4.09 (s, 2H), 3.78 (s, 5.1H), 3.67 (s, 1.4H), 2.44 (s, 2.1H) and 2.42 (s, 3H) ppm. ^{13}C NMR (176 MHz, DMSO-d_6) δ 171.54, 165.77, 159.56, 158.41, 154.44, 145.48, 142.52, 137.21, 136.95, 133.16, 133.14, 132.69, 132.62, 131.42, 131.34, 130.17, 129.94, 129.89, 127.76, 126.73, 126.70, 126.67, 126.35, 116.58, 116.54, 113.82, 110.91, 110.62, 105.96, 105.88, 102.57, 55.73, 37.94, 35.54, 19.90, and 19.53 ppm. Mass (ESI): m/z 448 [M + H]$^+$, 470 [M + Na]$^+$. Purity 99.4% (R_t = 23.51 min).

*(E/Z)-5-Methoxy-N-(4-(2-(2-(2-methoxybenzylidene)-hydrazineyl)-2-oxoethyl)thiazol-2-yl)-1H-indole-2-carboxamide (**6s**)*. White powder (Yield, 96%). Mp. 215 °C. FT-IR (KBr), ν (cm^{-1}): 3222, 2989, 2940, 2832, 1673, 1552, 1284, 1213, 1154, 887, and 750 cm^{-1}. ^{1}H NMR (700 MHz, DMSO-d_6) δ ^{1}H NMR (700 MHz, DMSO) δ 12.63 (s, 1H), 12.00 (s, 0.7H), 11.75 (s, 0.7H), 11.74 (s, 1H), 11.58 (s, 0.7H), 11.43 (s, 1H), 8.58 (s, 0.7H), 8.36 (s, 1H), 7.81 (t, J = 8.1 Hz, 1.7H), 7.57 (s, 1.7H), 7.44−7.35 (p, 1.7H), 7.37 (d, J = 8.9 Hz, 1.7H), 7.12 (d, J = 2.6 Hz, 2H), 7.10 (d, J = 8.7 Hz, 1.4H), 7.04 (s, 0.7H), 7.03−6.99 (m, 1.7H), 7.00 (s, 1H), 6.91 (dt, J = 8.9, 2.2 Hz, 1.7H), 4.09 (s, 2H), 3.87 (s, 2.1H), 3.85 (s, 3H), 3.78 (s, 5.1H), 3.64 (s, 1.4H) ppm. ^{13}C NMR (176 MHz, DMSO-d_6) δ ^{13}C NMR (176 MHz, DMSO) δ 171.53, 165.70, 159.55, 158.39, 158.14, 158.08, 158.01, 154.44, 145.58, 145.39, 142.39, 138.94, 133.16, 133.14, 131.98, 131.69, 129.95, 129.89, 127.76, 125.92, 125.75, 122.71, 122.64, 121.22, 116.58, 116.54, 113.81, 112.29, 112.27, 110.89, 110.60, 105.95, 105.87, 102.57, 56.18, 56.14, 55.72, 37.91, and 35.53 ppm. Mass (ESI): m/z 464[M + H]$^+$, 486 [M + Na]$^+$. Purity 98.4% (R_t = 16.33 min).

*(E/Z)-5-Methoxy-N-(4-(2-(2-(4-methoxybenzylidene)-hydrazineyl)-2-oxoethyl)thiazol-2-yl)-1H-indole-2-carboxamide (**6t**)*. White powder (Yield, 97%). Mp. 237 °C. FT-IR (KBr), ν (cm^{-1}): 3378, 3209, 2933, 2829, 1673, 1537, 1453, 1274, 1212, 929, 730, 430, and 415 cm^{-1}. ^{1}H NMR (700 MHz, DMSO-d_6) δ 12.62 (s, 1.75H), 11.73 (s, 0.75H), 11.72 (s, 1H), 11.43 (s, 0.75H), 11.31 (s, 1H), 8.15 (s, 1H), 7.94 (s, 1H), 7.63 (d, J = 7.1 Hz, 1.5H), 7.61 (d, J = 7.1 Hz, 2H), 7.56 (s, 1.75H), 7.34 (d, J = 9.0 Hz, 1.75H), 7.10 (s, 1.75H), 7.01 (d, J = 5.9 Hz, 1.75H), 6.99 (s, 1.75H), 6.98 (d, J = 6.9 Hz, 2H), 6.89 (d, J = 9.1 Hz, 1.75H), 4.06 (s, 2H), 3.79 (s, 2.25H), 3.78 (s, 3H), 3.76 (s, 5.25H) and 3.62 (s, 1.5H) ppm. ^{13}C NMR (176 MHz, DMSO-d_6) δ 171.39, 165.62, 161.25, 161.03, 159.51, 159.45, 158.33, 158.01, 154.44, 146.79, 145.72, 145.55, 143.18, 133.16, 133.13, 129.90, 129.85, 129.09, 128.78, 127.75, 127.30, 127.28, 116.58, 116.55, 114.79, 113.81, 110.81, 110.63, 105.95, 105.87, 102.56, 55.77, 55.76, 55.73, 37.91, and 35.49 ppm. Mass (ESI): m/z 464 [M + H]$^+$, 486 [M + Na]$^+$. Purity 97.2% (R_t = 22.01 min).

*(E/Z)-5-Methoxy-N-(4-(2-(2-(4-nitrobenzylidene)-hydrazineyl)-2-oxoethyl)thiazol-2-yl)-1H-indole-2-carboxamide (**6u**)*. Yellow powder (Yield, 98%). Mp. 258 °C. FT-IR (KBr), ν (cm^{-1}): 3276, 3202, 2987, 2822, 1655, 1630, 1585, 1544, 1519, 1455, 1426, 1390,1338, 1318, 1281, 1215, 1137, 1105, 1032, 942, 846, 735, 689, 544, and 450 cm^{-1}. ^{1}H NMR (700 MHz, DMSO-d_6) δ ^{1}H NMR (700 MHz, DMSO) δ 12.62 (s, 1.9H), 11.87 (s, 0.9H), 11.75 (s, 1H), 11.73 (s,

https://doi.org/10.1021/acsomega.4c06889
ACS Omega 2024, 9, 41944−41967

1.9H), ^{1}H NMR (700 MHz, DMSO) δ 12.62 (s, 2H), 11.87 (s, 1H), 11.75 (s, 1H), 11.73 (s, 2H), 8.32 (s, 0.9H), 8.27 (t, J = 11.6 Hz, 3.8H), 8.09 (s, 1H), 7.95 (t, J = 10.0 Hz, 3.8H), 7.55 (s, 1.9H), 7.34 (d, J = 10.3 Hz, 1.9H), 7.10 (s, 1.9H), 7.03 (s, 1.9H), 6.89 (d, J = 11.0 Hz, 1.9H), 4.12 (s, 2H), 3.76 (s, 5.4H) and 3.69 (s, 1.8H) ppm. ^{13}C NMR (176 MHz, DMSO-d_6) δ 170.96, 165.17, 159.41, 159.36, 158.21, 157.87, 154.35, 151.86, 151.67, 147.59, 145.78, 145.64, 144.02, 133.06, 133.04, 129.82, 129.78, 128.72, 128.38, 127.66, 122.02, 121.89, 116.45, 113.73, 112.23, 112.18, 110.63, 110.48, 105.85, 102.47, 55.63, 37.84, and 35.36 ppm. Mass (ESI): m/z 479 $[M + H]^+$, 517 $[M+K]^+$. Purity 97.7% (R_t = 28.33 min).

*(E/Z)-N-(4-(2-(2-(4-(Dimethylamino)benzylidene)-hydrazineyl)-2-oxoethyl)thiazol-2-yl)-5-methoxy-1H-indole-2-carboxamide (**6v**).* Pink powder (Yield, 99%). Mp. 257 °C. FT-IR (KBr), ν (cm^{-1}): 3447, 3387, 3203, 3047, 2826, 1683, 1656, 1614, 1538, 1453, 1363, 1275, 1216, 1185, 1120, 1066, 946,839, 813, and 724 cm^{-1}. ^{1}H NMR (700 MHz, DMSO-d_6) δ 12.64 (s, 1.85H), 11.75 (s, 0.85H), 11.74 (s, 1H), 11.28 (s, 0.85H), 11.17 (s, 1H), 8.08 (s, 0.85H), 7.88 (s, 1H), 7.58 (s, 1.85H), 7.52 (d, J = 8.8 Hz, 1.7H), 7.49 (d, J = 8.6 Hz, 1.85H), 7.37 (d, J = 9.5 Hz, 1.85H), 7.12 (s, 1.85H), 7.02 (s, 0.85H), 7.00 (s, 1H), 6.91 (d, J = 9.1 Hz, 2H), 6.76 (d, J = 8.6 Hz, 1.7H), 7.75 (d, J = 8.6 Hz, 2H), 4.06 (s, 2H), 3.78 (s, 5.55H), 3.62 (s, 1.7H), 2.98 (s, 5.1H) and 2.97 (s, 6H) ppm. ^{13}C NMR (176 MHz, DMSO-d_6) δ 171.05, 165.26, 159.5, 159.44, 158.30, 157.96, 154.44, 151.95, 151.76, 147.68, 145.87, 145.73, 144.11, 133.15, 133.13, 129.91, 129.86, 128.81, 128.47, 127.75, 122.11, 121.98, 116.58, 116.54, 113.81, 112.31, 112.27, 110.72, 110.57, 105.94, 105.86, 102.56, 55.72, 40.48, 37.92, and 35.45. ppm. Mass (ESI): m/z 447 $[M + H]^+$. Purity 97.5% (R_t = 24.70 min).

*(E/Z)-5-Methoxy-N-(4-(2-(2-(4-(methylthio)benzylidene)-hydrazineyl)-2-oxoethyl)thiazol-2-yl)-1H-indole-2-carboxamide (**6w**).* White powder (Yield, 96%). Mp. 257 °C. FT-IR (KBr), ν (cm^{-1}): 3344, 3215, 3148, 2985, 2833, 1663, 1542, 1406, 1281, 1269, 1212, 1159, 1120, 1038, 946, 812, 751, 718, 595, 544, 512, and 459 cm^{-1}. ^{1}H NMR (700 MHz, DMSO-d_6) δ 12.64 (s, 1.7H), 11.75 (s, 0.7H), 11.74 (s, 1H), 11.54 (s, 0.7H), 11.43 (s, 1H), 8.18 (s, 0.7H), 7.97 (s, 1H), 7.64 (d, J = 8.5 Hz, 1.4H), 7.62 (d, J = 8.5 Hz, 2H), 7.58 (s, 1.7H), 7.37 (d, J = 8.9 Hz, 1.7H), 7.32 (d, J = 8.5 Hz, 1.4H), 7.31 (d, J = 8.5 Hz, 2H), 7.12 (d, J = 2.7 Hz, 1.7H), 7.04 (s, 0.7H), 7.01 (s, 1H), 6.91 (dd, J = 8.9, 2.7 Hz, 1.7H), 4.09 (s, 2H), 3.78 (s, 5.1H), 3.66 (s, 1.4H), 2.52 (s, 2.1H) and 2.51 (s, 3H) ppm. ^{13}C NMR (176 MHz, DMSO-d_6) δ 171.53, 165.77, 159.52, 159.46, 158.36, 158.04, 154.44, 146.51, 145.64, 145.47, 142.93, 141.35, 140.99, 133.16, 133.14, 131.17, 129.90, 129.85, 127.92, 127.76, 127.64, 126.16, 126.11, 116.59, 116.55, 113.82, 110.86, 110.67, 105.96, 105.88, 102.57, 55.73, 37.91, 35.52, 14.76, and 14.72 ppm. Mass (ESI): m/z 480 $[M + H]^+$, 502 $[M + Na]^+$, 518 $[M+K]^+$. Purity 95.7% (R_t = 16.26 min).

*(E/Z)-N-(4-(2-(2-(3,4-Dichlorobenzylidene)hydrazineyl)-2-oxoethyl)thiazol-2-yl)-5-methoxy-1H-indole-2-carboxamide (**6x**).* White Colorless powder (Yield, 96%). Mp. 257 °C. FT-IR (KBr), ν (cm^{-1}): 3207, 3158, 2945, 2831, 1678, 1647, 1603, 1557, 1524, 1455, 1419, 1379, 1285, 1215, 1160, 1120, 1049, 1033, 927, 884, 839, 822, 799, 746, and 556 cm^{-1}. ^{1}H NMR (700 MHz, DMSO-d_6) δ 12.61 (s, 1H), 11.96 (s, 0.7H), 11.86 (s, 0.7H), 11.72 (s, 0.7H), 11.71 (s, 1H), 11.69 (s, 1H), 8.56 (s, 0.7H), 8.33 (s, 1H), 7.97 (d, J = 8.6 Hz, 1H), 7.94 (d, J = 8.5 Hz, 0.7H), 7.71 (d, J = 2.2 Hz, 0.7H), 7.70 (d, J = 2.2 Hz, 1H),7.55 (s, 1.7H), 7.49 (t, J = 9.0 Hz, 1.7H), 7.34 (d, J = 8.9 Hz, 1.7H), 7.10 (d, J = 2.6 Hz, 1.7H), 7.03 (s, 0.7H), 7.00 (s, 1H), 6.89 (dd, J = 8.9, 2.7 Hz, 1.7H), 4.09 (s, 2H), 3.76 (s, 5.1H) and 3.66 (s, 1.4H) ppm. ^{13}C NMR (176 MHz, DMSO-d_6) δ 171.86, 166.16, 159.54, 158.45, 158.18, 154.44, 145.32, 145.09, 141.81, 138.32, 135.52, 135.22, 134.23, 134.01, 133.16, 133.14, 131.07, 129.91, 129.84, 128.54, 128.48, 128.40, 127.76, 116.59, 116.56, 113.82, 111.06, 110.75, 105.98, 105.90, 102.56, 55.73, 37.94, and 35.56 ppm. Mass (ESI): m/z 502 $[^{35}(Cl)M+H]^+$, 504 $[^{37}(Cl)M+H]^+$. Purity 99.3% (R_t = 18.71 min).

*(E/Z)-N-(4-(2-(2-(2-Hydroxy-4-methoxybenzylidene)-hydrazineyl)-2-oxoethyl)thiazol-2-yl)-5-methoxy-1H-indole-2-carboxamide (**6y**).* Yellowish powder (Yield, 98%). Mp. 277 °C. FT-IR (KBr), ν (cm^{-1}): 3345, 3203, 3131, 2996, 2826, 1667, 1623, 1558, 1523, 1424, 1393, 1347, 1292, 1217, 1165, 1035, 949, 818, 789, 755, 741, and 536 cm^{-1}. ^{1}H NMR (700 MHz, DMSO-d_6) δ 12.61 (s, 1.4H), 11.73 (s, 1H), 11.71 (s, 0.4H), 11.68 (s, 1H), 11.45 (s, 1H), 11.29 (s, 0.4H), 10.20 (s, 0.4H), 8.32 (s, 1H), 8.19 (s, 0.4H), 7.55 (s, 1H), 7.53 (d, J = 8.7 Hz, 0.8H), 7.40 (d, J = 8.6 Hz, 1H), 7.34 (d, J = 9.0 Hz, 1.4H), 7.10 (s, 1.4H), 7.03 (s, 1H), 6.97 (s, 0.4H), 6.89 (dd, J = 8.9, 3.1 Hz, 1.4H), 6.50 (dd, J = 8.6, 2.2 Hz, 1H), 6.48 (d, J = 2.3 Hz, 0.4H), 6.46 (d, J = 2.3 Hz, 1H), 6.43 (d, J = 2.3 Hz, 0.4H), 4.01 (s, 0.8H), 3.76 (s, 6H), 3.76 (s, 1.2H), 3.73 (s, 1.2H) and 3.65 (s, 2H) ppm. ^{13}C NMR (176 MHz, DMSO-d_6) δ 170.89, 165.47, 162.48, 162.21, 159.73, 159.52, 158.40, 154.45, 147.98, 145.26, 141.97, 133.16, 131.50, 130.56, 129.84, 128.69, 127.75, 122.59, 116.59, 116.54, 113.82, 113.47, 112.14, 111.00, 110 58, 106.92, 106.89, 105.97, 105.89, 102.56, 101.60, 101.40, 55.79, 55.72, 37.62, and 35.73 ppm. Mass (ESI): m/z 480 $[M + H]^+$, 502 $[M + Na]^+$. Purity 98.9% (R_t = 16.05 min).

*(E/Z)-5-Methoxy-N-(4-(2-(2-(naphthalen-1-ylmethylene)-hydrazineyl)-2-oxoethyl)thiazol-2-yl)-1H-indole-2-carboxamide (**6z**).* Orange powder (Yield, 98%). Mp. 228 °C. FT-IR (KBr), ν (cm^{-1}): 3221, 3158, 3044, 2833, 1672, 1644, 1560, 1526, 1455, 1407, 1380, 1341, 1284, 1161, 1118, 1086, 1034, 943, 886, 828, 795, 770, 735, 553, 495, 459, and 427 cm^{-1}. ^{1}H NMR (700 MHz, DMSO-d_6) δ 12.63 (brs, 1H), 11.96 (brs, 0.7H), 11.74 (s, 0.7H), 11.72 (s, 1H), 11.66 (s, 0.7H), 11.51 (s, 1H), 8.83 (d, J = 8.8 Hz, 0.7H), 8.83 (s, 1H), 8.67 (s, 1H), 8.61 (d, J = 8.6 Hz, 1H), 8.01 (d, J = 6.8 Hz, 1.4H), 7.99 (d, J = 8.3 Hz, 2H), 7.88 (d, J = 6.8 Hz, 0.7H), 7.87 (d, J = 6.8 Hz, 1H), 7.64 (dddd, J = 8.4, 6.8, 2.9, 1.5 Hz, 1.7H), 7.61−7.56 (m, overlapped, 3.4H), 7.56 (m, overlapped, J = 3.0 Hz, 1.7H), 7.35 (d, J = 8.9 Hz, 0.7H), 7.34 (d, J = 8.9 Hz, 1H), 7.10 (d, J = 2.5 Hz, 1.7H), 7.07 (d, J = 0.9 Hz, 0.7H), 7.03 (d, J = 0.9 Hz, 1H), 6.89 (ddd, J = 8.9, 2.5, 1.6 Hz, 1.7H), 4.15 (s, 2H), 3.76 (s, 3H), 3.75 (s, 2.1H) and 3.71 (s, 0.7H) ppm. ^{13}C NMR (176 MHz, DMSO-d_6) δ 171.57, 165.92, 159.56, 158.45, 158.20, 154.44, 146.93, 145.48, 145.36, 143.30, 134.02, 134.00, 133.16, 133.14, 131.00, 130.73, 130.57, 130.48, 129.96, 129.93, 129.90, 129.31, 129.27, 128.53, 127.83, 127.81, 127.76, 126.78, 126.74, 126.08, 126.03, 124.79, 124.27, 116.58, 116.55, 113.81, 110.97, 110.68, 105.97, 105.90, 102.57, 55.72, 37.96, and 35.81 ppm. Mass (ESI): m/z 484 $[M + H]^+$, 506 $[M + Na]^+$. Purity 99.0% (R_t = 29.36 min).

General Procedure for the Preparation of 7. To the ethyl 2-(2-(1*H*-indole-2-carboxamido)thiazol-4-yl)acetate (**3a**) or Ethyl-2-(2-(5-methoxy-1*H*-indole-2-carboxamido)thiazol-4-yl)acetate (**3b**) (100 mg), 10% NaOH was added and was refluxed for 1h. Water was added. Addition of 5% $NaHCO_3$ solution gave white cake. Which was filtered, dried to obtain the desired product **7**.

https://doi.org/10.1021/acsomega.4c06889
ACS Omega 2024, 9, 41944−41967

*2-(2-(1H-Indole-2-carboxamido)thiazol-4-yl)acetic acid (**7a**).* White powder (Yield, 74%). Mp. 239 °C. FT-IR (KBr), ν (cm^{-1}): 3421, 3335, 3056, 1690, 1657, 1561, 1315, 1199, 1092, 1021, 973, 801, 744, and 581 cm^{-1}. ^{1}H NMR (700 MHz, DMSO-d_6) δ 12.70 (s, 1H), 12.40 (s, 1H), 11.87 (s, 1H), 7.66 (d, J = 8.1 Hz, 1H), 7.64 (s, 1H), 7.46 (d, J = 8.3 Hz, 1H), 7.24 (t, J = 7.7 Hz, 1H), 7.07 (t, J = 7.5 Hz, 1H), 7.01 (s, 1H) and 3.65 (s, 2H) ppm. ^{13}C NMR (176 MHz, DMSO-d_6) δ 172.12, 160.73, 158.09, 144.50, 137.78, 131.08, 127.45, 124.96, 122.64, 120.66, 112.95, 111.03, 106.24, and 37.36 ppm. Mass (ESI): m/z 302 $[M + H]^+$, 324 $[M + Na]^+$, 340 $[M + K]^+$.

*2-(2-(5-Methoxy-1H-indole-2-carboxamido)thiazol-4-yl)-acetic acid (**7b**).* Colorless powder (Yield, 76%). Mp. 218 °C. FT-IR (KBr), ν (cm^{-1}): 3364, 3099, 2927, 2836, 1654, 1636, 1557, 1541, 1522, 1507, 1457, 1338, 1283, 1213, 1158, 849, 750, 732, 727, 459, and 419 cm^{-1}. ^{1}H NMR (700 MHz, DMSO-d_6) δ 12.63 (d, J = 25.5 Hz, 1.8H), 11.73 (s, 1.8H), 10.60 (s, 1H), 8.79 (brs, 0.8H), 7.56 (s, 1.8H), 7.35 (d, J = 9.0 Hz, 1.8H), 7.11 (d, J = 2.7 Hz, 1.8H), 7.03 (s, 0.8H), 6.93 (s, 1H), 6.90 (ddd, J = 8.9, 2.5, 1.4 Hz, 1.8H) and 3.76 (s, 5.4H) ppm. ^{13}C NMR (176 MHz, DMSO-d_6) δ 170.57, 166.26, 159.54, 159.52, 158.43, 158.17, 154.45, 145.71, 144.27, 133.17, 133.15, 129.89, 129.82, 127.76, 116.61, 116.56, 113.82, 111.27, 110.53, 105.96, 105.94, 102.57, 55.73, 37.15, and 36.00 ppm.

General procedure for the preparation of 8. A mixture of KOH and hydroxylamine hydrochloride ($NH_2OH.HCl$) in MeOH was stirred in an ice bath for 1h to obtain a freshly prepared hydroxylamine (NH_2OH) solution in MeOH. To the ethyl 2-(2-(1*H*-indole-2-carboxamido)thiazol-4-yl)acetate (**3a**) or Ethyl-2-(2-(5-methoxy-1*H*-indole-2-carboxamido)thiazol-4-yl)acetate (**3b**) (100 mg), a freshly prepared hydroxylamine (NH_2OH) solution (3 mL) was added and the mixture was stirred for another 1h at room temperature. Solid white cake was filtered, dried to obtain the desired product.

*N-(4-(2-(Hydroxyamino)-2-oxoethyl)thiazol-2-yl)-1H-indole-2-carboxamide (**8a**).* Brown powder (Yield, 63%). Mp. 218 °C. FT-IR (KBr), ν (cm^{-1}): 3335, 3229, 3165, 3054, 2922, 1655, 1553, 1362, 1315, 1230, 1200, 1146, 975, 874, 744, 671, 581, and 433 cm^{-1}. ^{1}H NMR (700 MHz, DMSO-d_6) δ 12.70 (s, 1H), 12.67 (s, 1H), 11.87 (s, 2H), 10.60 (s, 1H), 8.84 (s, 1H), 7.66 (d, J = 7.7 Hz, 2H), 7.64 (s, 2H), 7.46 (d, J = 8.4 Hz, 2H), 7.25 (dd, J = 10.0, 4.7 Hz, 2H), 7.07 (p, J = 5.1, 3.7 Hz, 2H), 7.01 (s, 1H), 6.95 (s, 1H), 3.65 (s, 2H) and 3.39 (s, 2H) ppm. ^{13}C NMR (176 MHz, DMSO-d_6) δ 172.15, 166.34, 159.64, 158.26, 158.18, 145.64, 144.85, 137.77, 129.68, 127.43, 125.00, 122.64, 120.70, 112.95, 111.03, 110.63, 106.28, 106.26, 37.34, and 35.96 ppm. Mass (ESI): m/z 317 $[M + H]^+$, 339 $[M + Na]^+$.

*N-(4-(2-(Hydroxyamino)-2-oxoethyl)thiazol-2-yl)-5-methoxy-1H-indole-2-carboxamide (**8b**).* White powder (Yield, 52%). Mp. 235 °C. FT-IR (KBr), ν (cm^{-1}): 3428, 3326, 3106, 2924, 2848, 2585, 1707, 1684, 1604, 1560, 1520, 1376, 1319, 1228, 1210, 1180, 1033, 796, 750, 727, and 459 cm^{-1}. ^{1}H NMR (700 MHz, DMSO-d_6) δ 12.64 (s, 1H), 11.73 (s, 1H), 7.56 (d, J = 2.5 Hz, 1H), 7.35 (d, J = 8.8 Hz, 1H), 7.11 (d, J = 2.6 Hz, 1H), 7.00 (s, 1H), 6.89 (dd, J = 8.8, 2.5 Hz, 1H), 3.76 (s, 3H) and 3.64 (s, 2H) ppm. ^{13}C NMR (176 MHz, DMSO-d_6) δ 172.11, 159.55, 158.30, 154.45, 144.80, 133.16, 129.89, 127.75, 116.58, 113.83, 110.96, 105.93, 102.57, 55.73, and 37.34 ppm. Mass (ESI): m/z 346 $[M + H]^+$.

Biological Evaluation. *In-vitro Cytotoxicity Assay of **6**–**8**.* The cytotoxicity assay of compounds along with reference compounds, was conducted using the colorimetric MTT assay. The assay was performed on multiple cancer cell lines and one normal cell line, following a previously reported method.[120,121] In brief, the cells were cultured in 96-well plates with a density of 1.0×10^4 cells per well, supplemented with 10% fetal bovine serum (FBS), an antibiotic cocktail of streptomycin (100 μg/mL) and penicillin (100 units/mL), and RPMI 11640 medium. The plates were then incubated for 48 h at 37 °C, 5% CO_2, and 100% relative humidity. Afterward, the cells were treated with increasing concentrations of the synthesized compounds, as well as sunitinib, and further incubated for 24 h. Following the incubation period, 20 μL of MTT solution was added to each well and left in the incubator for 4 h to allow formazan formation. Subsequently, 100 μL of dimethyl sulfoxide was added to dissolve the insoluble formazan. Finally, the absorbance of the samples was measured at 570 nm using a BioTek EXL 800 plate reader (Agilent Technologies, Inc., Santa Clara, CA, USA). The relative cell viability percentage was calculated as (A570 of treated samples/A570 of untreated sample) × 100.

*In-vitro Enzyme Assays of **6e**, **6i**, **6q**, **6v**, **7a**, and **7b**.* Fifteen derivatives of the synthesized compounds were evaluated for their inhibitory activities against EGFR, VEGFR-2, Her2, and CDK2 using specific human ELISA kits, as described in the referenced methods.[120,121] In the assay, various concentrations of the synthesized compounds were added to a 96-well plate, along with specific antibodies for each kinase enzyme. The plate was then incubated at room temperature for 2.5 h to allow binding of the compounds to the respective enzyme targets. After the incubation period, the 96-well plate was washed to remove any unbound components. Subsequently, 100 μL of an in-house prepared biotin antibody was added to each well and incubated at ambient temperature for 1 h. Following another wash step, 100 μL of streptavidin solution was added to each well and left to incubate for 45 min at ambient temperature. After a final wash, 100 μL of 3,3′,5,5′-tetramethylbenzidine (TMB) substrate reagent was applied to initiate a colorimetric reaction, and the plate was incubated at ambient temperature for 30 min. Finally, 50 μL of a stop solution was added to halt the reaction, and the absorbance was directly measured at 450 nm. To determine the concentrations of the compounds, a standard curve was constructed by plotting concentration values on the X-axis and corresponding absorbance values on the Y-axis.

*Cell Cycle Analysis of **6i** and **6v**.* To assess the impact of the synthesized compounds **6i** and **6v** on cell cycle distribution, the ab139418 Propidium Iodide flow cytometry kit/BD was utilized. The experimental procedure involved the following steps: First, MCF-7 cells were cultured in 6-well plates with a density of 2×10^5 cells per well. The cells were allowed to incubate for 24 h to establish their growth.[120,121] Subsequently, the cells were treated with the selected compounds at concentrations corresponding to their IC_{50} values. The treatment was continued for an additional 24 h. To fix the treated MCF-7 cells, a solution of 70% ethanol was applied, and the mixture was incubated for 12 h at 4 °C. Following fixation, the wells were washed with cold PBS. Then, 100 μL of RNase A was added and incubated for 30 min at 37 °C. The cells were further stained with Propidium Iodide (400 μL) in a dark environment at room temperature for an additional 30 min. The labeled cells were identified using the Epics XLMCL flow cytometer equipment from Beckman Coulter, located in Apeldoorn, Netherlands. Finally, the

https://doi.org/10.1021/acsomega.4c06889
ACS Omega 2024, 9, 41944−41967

obtained experimental results were analyzed using Flowing software (version 2.5.1, Turku Centre for Biotechnology, Turku, Finland) for further data interpretation and analysis.

*Annexin-V/propidium Iodide (PI) Double Staining Assay of **6i** and **6v**.* In order to assess the apoptotic effect of the synthesized compounds **6i** and **6v**, MCF-7 cells were cultured in triplicate at a density of 2.0×10^5 cells per well. Subsequently, the cells were treated with the compounds at their respective IC_{50} values, which were determined through the MTT assay.[120,121] After a 24-h incubation period, the cells were detached using trypsin, collected, and then centrifuged. The cell pellet was washed twice with PBS and suspended in 0.1 mL of binding buffer. The cells were then dual-stained with Annexin V-FITC (5 μL) and propidium iodide (5 μL) in a dark environment, allowing for a 15 min incubation at room temperature. Flow cytometry analysis was performed using the Epics XL-MCL flow cytometry equipment from Beckman Coulter, located in Apeldoorn, Netherlands. The equipment utilized an excitation wavelength of 488 nm and an emission wavelength of 530 nm. Finally, the experimental results were analyzed using Flowing software (version 2.5.1, Turku Centre for Biotechnology, Turku, Finland) to interpret and analyze the obtained data from the experiment.

*Determination of apoptotic protein levels of **6i** and **6v** using Real-time Polymerase Chain Reaction (PCR). RNA Isolation and Reverse Transcription.* mRNA isolation was performed using the RNeasy extraction kit. Up to 1×10^7 cells, depending on the cell line, were disrupted in Buffer RLT and homogenized. Ethanol was added to the lysate, creating conditions that facilitated selective binding of RNA to the RNeasy membrane. The lysate was then applied to the RNeasy Mini spin column, where total RNA bound to the membrane while contaminants were efficiently washed away. Finally, high-quality RNA was eluted from the membrane using RNase-free water. All binding, washing, and elution steps were carried out using centrifugation in a microcentrifuge (Invitrogen Life Technologies, Carlsbad, CA, USA). To ensure the removal of any residual DNA, the RNA samples were treated with the Turbo DNA-free kit (Ambion Inc., Foster, CA, USA). Subsequently, first-strand complementary DNA (cDNA) synthesis was performed using 2 μg of total RNA and the Superscript First-Strand Synthesis System (Invitrogen Inc.). For cDNA synthesis, the RNA template and reverse oligonucleotide primers (25 pmol of each) were denatured at 70 °C for 10 min. Then, 40 U of reverse transcriptase was added to the reaction mixture, along with RT buffer (50 mM KCl, 20 mM Tris−HCl, pH 8.4), a dNTP mix (250 μM each), 40 U of RNase inhibitor, and RNase-free water to reach the final volume. The reaction mixture (50 μL) was incubated at 43 °C for 1 h, followed by immediate cooling at 4 °C. The resulting cDNA was either used immediately for PCR or stored at −80 °C until further use.

Quantitative Real-Time PCR. The real-time PCR experiments were performed using an ABI Prism 7500 Sequence Detection System (Applied Biosystems, Foster City, CA, USA) and the Power SYBR Green Master Mix kit (Invitrogen Life Technologies). All PCR procedures were conducted in a dedicated room, and strict precautions were taken, including the use of gloves, face masks, and barrier tips. In each experiment, the samples were run in duplicate on 96-well optical PCR plates, with a final reaction volume of 25 μL. The PCR cycling parameters consisted of an initial cycle at 50 °C for 2 min, followed by a cycle at 95 °C for 10 min, and then 40 cycles at 95 °C for 15 s and 60 °C for 1 min. Specific primers for caspase-3, caspase-8, bcl-2, bax, and glyceraldehyde-3-phosphate dehydrogenase (GAPDH) were used for PCR amplification. The GAPDH gene was chosen as a reference gene for normalizing the expression of target genes due to its involvement in the glycolysis pathway of cells. The primer sequences were designed based on the sequences obtained from GenBank using the Blast program (http://www.ncbi.nlm.nih.gov/blast/blast.cgi). To ensure specificity and sensitivity, all primer sequences were further analyzed using the Integrated DNA Technologies Web site program. By following these procedures, we aimed to accurately quantify the expression levels of caspase-3, caspase-8, bcl-2, and bax apoptotic genes, while normalizing the results to the GAPDH reference gene. This approach ensured reliable and precise analysis of apoptotic protein levels using real-time PCR (Table 8).

Table 8. Selected PCR Primers used in Real-Time PCR for Apoptosis-Related Genes and Normalizer Gene GAPDH

Name	Sequence (5̀ 3̀)	Fragment length (pb)
HsGAPDH-F1(sense)	TTCCAGGACCAAGATCCCTCCAAA	24
HsGAPDH-R2 (antisense)	ATGGTGGTGAAGACACCAGTGAAC	24
HsCasp3F (sense)	TGCATACTCCACAGCACCTGGTTA	24
HsCasp3Rev (antisense)	CATGGCACAAAGCGACTGGATGAA	24
HsCasp8F (sense)	TTTCACTGTGTTAGCCAGGGTGGTA	25
HsCasp8Rev (antisense)	CCTGTAATCCCAGCACTTTGGGAG	24
HsBcl-2F (sense)	ATGACCAGACACTGACCATCCACT	24
HsBcl-2Rev (antisense)	ATGTAGTGGTTCTCCTGGTGGCAA	24
HsBAXF (sense)	TCTACTTTGCCAGCAAACTGGTGC	24
HsBAXRev (antisense)	TGTCCAGCCCATGATGGTTCTGAT	24

In-silico Studies of 6i and 6v. *Molecular Docking of **6i** and **6v**.* Compound structures for molecules **6i** and **6v** were drawn using ChemOffice's ChemDraw 16.0 tool, ensuring proper 2D orientation. The 3D structure of Roscovitine, sorafenib, lapatinib, dasatinib and gefitinib were downloaded from pubchem. To optimize their energy, all molecules underwent minimization using ChemBio3D. X-ray crystal structures of the main kinase domains complexed with other molecules (HER2: PDB id = 3pp0, VEGFR2: PDB id = 4ASD, EGFR: PDB id = 3POZ, CDK2: PDB id = 1HCK) were retrieved from the RCSB Protein Data Bank. Using PyMOL software (version 2.5.2), hetero atoms, water molecules, and inhibitors present in the structures were removed.[122] The Swiss-PDB Viewer software (version 4.1.0) was utilized to optimize and validate the crystal structures of the receptors based on their lowest energy states. Docking studies were performed using Autodock Vina[123] with the assistance of UCSF Chimera.[124] The previously minimized domains and ligands were used as input for Autodock Vina. Before docking, hydrogens and Gasteiger charges were added to the ligands. The active site of the main domain was targeted to generate a grid box in Autodock Vina. After docking, Discovery Studio Visualizer and UCSF Chimera X were employed to visualize

https://doi.org/10.1021/acsomega.4c06889
ACS Omega 2024, 9, 41944−41967

the interactions. The ligands were represented in different colors, and hydrogen bonds and interacting residues were displayed in a ball-and-stick model representation.

In-silico ADME Studies of the Compounds. To conduct *in-silico* ADME (Absorption, Distribution, Metabolism, and Excretion) analysis, the structures of all compounds were processed using the LigPrep module within the Schrödinger Maestro software. LigPrep ensures that the compounds are optimized and suitable for further analysis.[120,121] Subsequently, the ADME properties of the compounds were calculated using the QikProp module, also part of the Schrödinger Maestro software package. QikProp employs advanced computational models and algorithms to predict essential ADME parameters, including aqueous solubility, lipophilicity (logP), blood-brain barrier penetration, and more. By employing LigPrep and QikProp, the molecular structures of the compounds were carefully prepared, and their ADME properties were accurately predicted. This valuable information assists in evaluating the compounds' pharmacokinetic profiles and aids in the assessment of their potential as drug candidates.[125]

■ ASSOCIATED CONTENT

Supporting Information

The Supporting Information is available free of charge at https://pubs.acs.org/doi/10.1021/acsomega.4c06889.

Supporting data (NMR, IR, Mass) data are available online (PDF)

■ AUTHOR INFORMATION

Corresponding Authors

Reem I. Al-Wabli − *Department of Pharmaceutical Chemistry, College of Pharmacy, King Saud University, Riyadh 11451, Saudi Arabia*; Email: ralwabli@ksu.edu.sa

A. F. M. Motiur Rahman − *Department of Pharmaceutical Chemistry, College of Pharmacy, King Saud University, Riyadh 11451, Saudi Arabia*; orcid.org/0000-0002-5807-5625; Email: afmrahman@ksu.edu.sa

Authors

Njood M. Saadan − *Department of Pharmaceutical Chemistry, College of Pharmacy, King Saud University, Riyadh 11451, Saudi Arabia*

Wahid U. Ahmed − *School of Pharmaceutical Sciences, Zhengzhou University, Zhengzhou, Henan 450001, China*

Adnan A. Kadi − *Department of Pharmaceutical Chemistry, College of Pharmacy, King Saud University, Riyadh 11451, Saudi Arabia*

Maha S. Al-Mutairi − *Department of Pharmaceutical Chemistry, College of Pharmacy, King Saud University, Riyadh 11451, Saudi Arabia*

Complete contact information is available at: https://pubs.acs.org/10.1021/acsomega.4c06889

Author Contributions

Conceptualization, R.I.A-W. and A.F.M.M.R.; methodology, N.M.S. and W.U.A.; validation, R.I.A-W. and A.F.M.M.R.; formal analysis, N.M.S. and A.F.M.M.R.; investigation, R.I.A.-W., M.S.A.-M. and A.F.M.M.R.; resources, A.A.K, R.I.A.-W. and A.F.M.M.R.; data curation, N.M.S. and W.U.A.; writing—original draft preparation, A.F.M.M.R.; writing—review and editing, N.M.S. and W.U.A., R.I.A-W. and A.F.M.M.R.; supervision, R.I.A.-W. and A.F.M.M.R.; funding acquisition, R.I.A.-W. All authors have read and agreed to the published version of the manuscript.

Funding

This work was funded by the "Researchers Supporting Project number (RSP2024R207), King Saud University, Riyadh, Saudi Arabia".

Notes

The authors declare no competing financial interest.

■ ACKNOWLEDGMENTS

The authors extend their appreciation to the Researchers Supporting Project number (RSP2024R207), King Saud University, Riyadh, Saudi Arabia for funding this work.

■ REFERENCES

(1) Siegel, R. L.; Miller, K. D.; Wagle, N. S.; Jemal, A. Cancer statistics, 2023. *Ca Cancer J. Clin* **2023**, *73* (1), 17−48.

(2) Alessy, S. A.; AlWaheidi, S. Moving cancer prevention and care forward in Saudi Arabia. *Journal of Cancer Policy* **2020**, *26*, No. 100250.

(3) Alkhudair, N.; Alshamrani, M.; Samarkandi, H.; Almodaheem, H.; Alabdulkarim, H.; Alsaqaaby, M.; Alnajjar, F.; Alhashem, H.; Bakkar, M.; Bazarbashi, S.; Alnahedh, M.; Alfraih, F.; Alawagi, M.; Al-jedai, A. Cancer Management in Saudi Arabia: Recommendations by the Saudi Oncology HeAlth Economics ExpeRt GrouP (SHARP). *Saudi Pharmaceutical Journal* **2021**, *29* (2), 115−120.

(4) Anand, P.; Kunnumakara, A. B.; Sundaram, C.; Harikumar, K. B.; Tharakan, S. T.; Lai, O. S.; Sung, B.; Aggarwal, B. B. Cancer is a preventable disease that requires major lifestyle changes. *Pharm. Res.* **2008**, *25* (9), 2097−2116.

(5) Choi, J. W.; Hua, T. N. M. Impact of Lifestyle Behaviors on Cancer Risk and Prevention. *J. Lifestyle Med.* **2021**, *11* (1), 1−7.

(6) Rumgay, H.; Shield, K.; Charvat, H.; Ferrari, P.; Sornpaisarn, B.; Obot, I.; Islami, F.; Lemmens, V. E. P. P.; Rehm, J.; Soerjomataram, I. Global burden of cancer in 2020 attributable to alcohol consumption: a population-based study. *Lancet Oncology* **2021**, *22* (8), 1071−1080.

(7) Scherübl, H. Tobacco Smoking and Gastrointestinal Cancer Risk. *Visc Med.* **2022**, *38* (3), 217−222.

(8) Pothiwala, P.; Jain, S. K.; Yaturu, S. Metabolic syndrome and cancer. *Metab Syndr Relat Disord* **2009**, *7* (4), 279−88.

(9) Moten, A.; Schafer, D.; Farmer, P.; Kim, J.; Ferrari, M. Redefining global health priorities: Improving cancer care in developing settings. *J. Glob Health* **2014**, *4* (1), No. 010304.

(10) Alzahrani, S.; Al Doghaither, H.; Al-Ghafari, A. General insight into cancer: An overview of colorectal cancer (Review). *Mol. Clin. Oncol.* **2021**, *15* (6), 271.

(11) Kocarnik, J. M.; Compton, K.; Dean, F. E.; Fu, W.; Gaw, B. L.; Harvey, J. D.; Henrikson, H. J.; Lu, D.; Pennini, A.; Xu, R.; Ababneh, E. Cancer Incidence, Mortality, Years of Life Lost, Years Lived With Disability, and Disability-Adjusted Life Years for 29 Cancer Groups From 2010 to 2019: A Systematic Analysis for the Global Burden of Disease Study 2019. *JAMA Oncol.* **2022**, *8* (3), 420−444.

(12) Ryszkiewicz, P.; Malinowska, B.; Schlicker, E. Polypharmacology: promises and new drugs in 2022. *Pharmacological Reports* **2023**, *75* (4), 755−770.

(13) Agis-Torres, A.; Sollhuber, M.; Fernandez, M.; Sanchez-Montero, J. M. Multi-Target-Directed Ligands and other Therapeutic Strategies in the Search of a Real Solution for Alzheimer's Disease. *Curr. Neuropharmacol.* **2014**, *12* (1), 2−36.

(14) Hanselmann, R. G.; Welter, C. Origin of Cancer: Cell work is the Key to Understanding Cancer Initiation and Progression. *Front Cell Dev Biol.* **2022**, *10*, No. 787995.

(15) Mendiratta, G.; Ke, E.; Aziz, M.; Liarakos, D.; Tong, M.; Stites, E. C. Cancer gene mutation frequencies for the U.S. population. *Nat. Commun.* **2021**, *12* (1), 5961.

(16) Iqbal, N.; Iqbal, N. Human Epidermal Growth Factor Receptor 2 (HER2) in Cancers: Overexpression and Therapeutic Implications. *Mol. Biol. Int.* **2014**, *2014*, 852748.
(17) Alhmoud, J. F.; Woolley, J. F.; Al Moustafa, A. E.; Malki, M. I. DNA Damage/Repair Management in Cancers. *Cancers* **2020**, *12* (4), 309.
(18) Bielski, C. M.; Taylor, B. S. Homing in on genomic instability as a therapeutic target in cancer. *Nat. Commun.* **2021**, *12* (1), 3663.
(19) Guo, Y.; Pan, W.; Liu, S.; Shen, Z.; Xu, Y.; Hu, L. ERK/MAPK signalling pathway and tumorigenesis. *Exp. Ther. Med.* **2020**, *19* (3), 1997−2007.
(20) He, Y.; Sun, M. M.; Zhang, G. G.; Yang, J.; Chen, K. S.; Xu, W. W.; Li, B. Targeting PI3K/Akt signal transduction for cancer therapy. *Signal Transduction Targeted Ther.* **2021**, *6* (1), 425.
(21) Yip, H. Y. K.; Papa, A. Signaling Pathways in Cancer: Therapeutic Targets, Combinatorial Treatments, and New Developments. *Cells* **2021**, *10* (3), 659.
(22) Fass, L. Imaging and cancer: a review. *Mol. Oncol* **2008**, *2* (2), 115−52.
(23) Carovac, A.; Smajlovic, F.; Junuzovic, D. Application of ultrasound in medicine. *Acta Inform Med.* **2011**, *19* (3), 168−71.
(24) Hamilton, B., 5 - Diagnostic Imaging. In *Oral, Head and Neck Oncology and Reconstructive Surgery*, Bell, R. B.; Fernandes, R. P.; Andersen, P. E., Eds. Elsevier: 2018; pp 107−118.
(25) Li, R.; Zheng, J.; Wang, Y.; Bai, W.; Lu, Y.; Geng, J.; Feng, J.; Wang, N.; Zhao, Y.; Wang, J. A novel nitroreductase-responsive turn-off fluorescent probe based on AIEgen and its bioimaging application. *J. Mol. Struct.* **2023**, *1294*, No. 136483.
(26) Woo, Y.; Chaurasiya, S.; O'Leary, M.; Han, E.; Fong, Y. Fluorescent imaging for cancer therapy and cancer gene therapy. *Molecular Therapy - Oncolytics* **2021**, *23*, 231−238.
(27) Kellert, M.; Hoppenz, P.; Lönnecke, P.; Worm, D. J.; Riedl, B.; Koebberling, J.; Beck-Sickinger, A. G.; Hey-Hawkins, E. Tuning a modular system - synthesis and characterisation of a boron-rich s-triazine-based carboxylic acid and amine bearing a galactopyranosyl moiety. *Dalton Trans* **2020**, *49* (1), 57−69.
(28) Coghi, P.; Fazal, T.; Hosmane, N. S.; Zhu, Y. Diagnostic and theranostic technologies used in boron neutron capture therapy − A brief review. *Inorg. Chem. Commun.* **2024**, *159*, No. 111698.
(29) Gabel, D., Safety and Efficacy in Boron Neutron Capture Therapy. In *Boron Neutron Capture Therapy: Toward Clinical Trials of Glioma Treatment*, Gabel, D.; Moss, R., Eds. Springer: US: Boston, MA, 1992; pp 7−13.
(30) Locher, G. I. Biological effects and therapeutic possibilities of neutrons. *Am. J. Roentgenol. Radium Ther* **1936**, *36*, 1−18.
(31) Maisy, D. L. B. D. W. T. P. E. V. M. N. *Positron Emission Tomography: Basic Sciences*. Springer-Verlag: Secaucus, NJ, 2005.
(32) Yang, W.; Zhong, Z.; Feng, G.; Wang, Z. Advances in positron emission tomography tracers related to vascular calcification. *Ann. Nucl. Med.* **2022**, *36* (9), 787−797.
(33) Nagpal, M.; Singh, S.; Singh, P.; Chauhan, P.; Zaidi, M. A. Tumor markers: A diagnostic tool. *Natl. J. Maxillofac Surg* **2016**, *7* (1), 17−20.
(34) Bruns, J.; Delling, G.; Henne-Bruns, D.; Hossfeld, D. K. Biopsy of tumors of the musculoskeletal system. *Dtsch. Arztebl. Int.* **2008**, *105* (27), 492.
(35) Liu, J. C.; Ridge, J. A., Chapter 67 - What is Cancer? In *Abernathy's Surgical Secrets*(Seventh ed.),Harken, A. H.; Moore, E. E., Eds. Elsevier:2018; pp 307−310.
(36) Lee, A. W. M.; Zong, J. F.; Pan, J. J.; Choi, H. C. W.; Sze, H. C. K., Chapter 9 - Staging of Nasopharyngeal Carcinoma Based on the 8th ed. of the AJCC/UICC Staging System. In *Nasopharyngeal Carcinoma*, Lee, A. W. M.; Lung, M. L.; Ng, W. T., Eds. Academic Press: 2019; pp 179−203.
(37) Baskar, R.; Lee, K. A.; Yeo, R.; Yeoh, K. W. Cancer and radiation therapy: current advances and future directions. *Int. J. Med. Sci.* **2012**, *9* (3), 193−9.
(38) Endo, M.; Lin, P. P. Surgical margins in the management of extremity soft tissue sarcoma. *Chinese Clinical Oncology* **2018**, *7* (4), 37.
(39) Anand, U.; Dey, A.; Chandel, A. K. S.; Sanyal, R.; Mishra, A.; Pandey, D. K.; De Falco, V.; Upadhyay, A.; Kandimalla, R.; Chaudhary, A.; Dhanjal, J. K.; Dewanjee, S.; Vallamkondu, J.; Pérez de la Lastra, J. M. Cancer chemotherapy and beyond: Current status, drug candidates, associated risks and progress in targeted therapeutics. *Genes & Diseases* **2023**, *10* (4), 1367−1401.
(40) Sahu, M.; Suryawanshi, H. Immunotherapy: The future of cancer treatment. *J. Oral Maxillofac Pathol* **2021**, *25* (2), 371.
(41) Shuel, S. L. Targeted cancer therapies: Clinical pearls for primary care. *Can. Fam Physician* **2022**, *68* (7), 515−518.
(42) Abraham, J.; Staffurth, J. Hormonal therapy for cancer. *Medicine* **2016**, *44* (1), 30−33.
(43) Krzyszczyk, P.; Acevedo, A.; Davidoff, E. J.; Timmins, L. M.; Marrero-Berrios, I.; Patel, M.; White, C.; Lowe, C.; Sherba, J. J.; Hartmanshenn, C.; O'Neill, K. M.; Balter, M. L.; Fritz, Z. R.; Androulakis, I. P.; Schloss, R. S.; Yarmush, M. L. The growing role of precision and personalized medicine for cancer treatment. *Technology* **2018**, *6* (3−4), 79−100.
(44) Naithani, N.; Sinha, S.; Misra, P.; Vasudevan, B.; Sahu, R. Precision medicine: Concept and tools. *Med. J. Armed Forces India* **2021**, *77* (3), 249−257.
(45) Weigmann, K. Releasing the brakes to fight cancer: The recent discovery of checkpoints has boosted the field of cancer immunotherapy. *EMBO Rep* **2016**, *17* (9), 1257−60.
(46) Sterner, R. C.; Sterner, R. M. CAR-T cell therapy: current limitations and potential strategies. *Blood Cancer J.* **2021**, *11* (4), 69.
(47) Supuran, C. T.; Scozzafava, A. Protein tyrosine kinase inhibitors as anticancer agents. *Expert Opinion on Therapeutic Patents* **2004**, *14* (1), 35−53.
(48) Traxler, P. Tyrosine kinases as targets in cancer therapy - successes and failures. *Expert Opin Ther Targets* **2003**, *7* (2), 215−34.
(49) Bhullar, K. S.; Lagarón, N. O.; McGowan, E. M.; Parmar, I.; Jha, A.; Hubbard, B. P.; Rupasinghe, H. P. V. Kinase-targeted cancer therapies: progress, challenges and future directions. *Mol. Cancer* **2018**, *17* (1), 48.
(50) Alkahtani, H. M.; Abdalla, A. N.; Obaidullah, A. J.; Alanazi, M. M.; Almehizia, A. A.; Alanazi, M. G.; Ahmed, A. Y.; Alwassil, O. I.; Darwish, H. W.; Abdel-Aziz, A. A.; El-Azab, A. S. Synthesis, cytotoxic evaluation, and molecular docking studies of novel quinazoline derivatives with benzenesulfonamide and anilide tails: Dual inhibitors of EGFR/HER2. *Bioorg Chem.* **2020**, *95*, No. 103461.
(51) Abbas, S. E.; Aly, E. I.; Awadallah, F. M.; Mahmoud, W. R. 4-Substituted-1-phenyl-1H-pyrazolo[3,4-d]pyrimidine derivatives: design, synthesis, antitumor and EGFR tyrosine kinase inhibitory activity. *Chem. Biol. Drug Des* **2015**, *85* (5), 608−22.
(52) Baak, J. P. A.; Li, H.; Guo, H. Clinical and Biological Interpretation of Survival Curves of Cancer Patients, Exemplified With Stage IV Non-Small Cell Lung Cancers With Long Follow-up. *Front Oncol* **2022**, *12*, No. 837419.
(53) Alsaif, N. A.; Taghour, M. S.; Alanazi, M. M.; Obaidullah, A. J.; Alanazi, W. A.; Alasmari, A.; Albassam, H.; Dahab, M. A.; Mahdy, H. A. Identification of new [1,2,4]triazolo[4,3-a]quinoxalines as potent VEGFR-2 tyrosine kinase inhibitors: Design, synthesis, anticancer evaluation, and in silico studies. *Bioorg. Med. Chem.* **2021**, *46*, No. 116384.
(54) Alsaif, N. A.; Elwan, A.; Alanazi, M. M.; Obaidullah, A. J.; Alanazi, W. A.; Alasmari, A. F.; Albassam, H.; Mahdy, H. A.; Taghour, M. S. Design, synthesis and molecular docking of new [1,2,4]triazolo[4,3-a]quinoxaline derivatives as anticancer agents targeting VEGFR-2 kinase. *Mol. Divers* **2022**, *26* (4), 1915−1932.
(55) Malumbres, M. Cyclin-dependent kinases. *Genome Biol.* **2014**, *15* (6), 122.
(56) Ivasechko, I.; Yushyn, I.; Roszczenko, P.; Senkiv, J.; Finiuk, N.; Lesyk, D.; Holota, S.; Czarnomysy, R.; Klyuchivska, O.; Khyluk, D.; Kashchak, N.; Gzella, A.; Bielawski, K.; Bielawska, A.; Stoika, R.;

https://doi.org/10.1021/acsomega.4c06889
ACS Omega 2024, 9, 41944−41967

Lesyk, R. Development of Novel Pyridine-Thiazole Hybrid Molecules as Potential Anticancer Agents. *Molecules* **2022**, *27* (19), 6219.
(57) Sharma, D.; Singh, M.; Joshi, J.; Garg, M.; Chaudhary, V.; Blankenberg, D.; Chandna, S.; Kumar, V.; Rani, R. Design and Synthesis of Thiazole Scaffold-Based Small Molecules as Anticancer Agents Targeting the Human Lactate Dehydrogenase A Enzyme. *ACS Omega* **2023**, *8* (20), 17552−17562.
(58) Bathula, S.; Sankaranarayanan, M.; Malgija, B.; Kaliappan, I.; Bhandare, R. R.; Shaik, A. B. 2-Amino Thiazole Derivatives as Prospective Aurora Kinase Inhibitors against Breast Cancer: QSAR, ADMET Prediction, Molecular Docking, and Molecular Dynamic Simulation Studies. *ACS Omega* **2023**, *8* (46), 44287−44311.
(59) Salem, M. G.; El-Maaty, D. M. A.; El-Deen, Y. I. M.; Elesawy, B. H.; Askary, A. E.; Saleh, A.; Saied, E. M.; Behery, M. E. Novel 1,3-Thiazole Analogues with Potent Activity against Breast Cancer: A Design, Synthesis, In Vitro, and In Silico Study. *Molecules* **2022**, *27* (15), 4898.
(60) Traer, E.; Deininger, M. W. How much and how long: tyrosine kinase inhibitor therapy in chronic myeloid leukemia. *Clin Lymphoma Myeloma Leuk* **2010**, *10* (Suppl 1), S20−S26.
(61) Taruneshwar Jha, K.; Shome, A.; Chahat; Chawla, P. A. Recent advances in nitrogen-containing heterocyclic compounds as receptor tyrosine kinase inhibitors for the treatment of cancer: Biological activity and structural activity relationship. *Bioorganic Chemistry* **2023**, *138*, No. 106680.
(62) Le Tourneau, C.; Raymond, E.; Faivre, S. Sunitinib: a novel tyrosine kinase inhibitor. A brief review of its therapeutic potential in the treatment of renal carcinoma and gastrointestinal stromal tumors (GIST). *Ther Clin Risk Manag* **2007**, *3* (2), 341−8.
(63) Papaetis, G. S.; Syrigos, K. N. Sunitinib: a multitargeted receptor tyrosine kinase inhibitor in the era of molecular cancer therapies. *BioDrugs* **2009**, *23* (6), 377−89.
(64) Villegas, C.; González-Chavarría, I.; Burgos, V.; Iturra-Beiza, H.; Ulrich, H.; Paz, C. Epothilones as Natural Compounds for Novel Anticancer Drugs Development. *Int. J. Mol. Sci.* **2023**, *24* (7), 6063.
(65) Cooney, D. A.; Jayaram, H. N.; Glazer, R. I.; Kelley, J. A.; Marquez, V. E.; Gebeyehu, G.; Van Cott, A. C.; Zwelling, L. A.; Johns, D. G. Studies on the mechanism of action of tiazofurin metabolism to an analog of NAD with potent IMP dehydrogenase-inhibitory activity. *Adv. Enzyme Regul* **1983**, *21*, 271−303.
(66) Devi, N.; Kaur, K.; Biharee, A.; Jaitak, V. Recent Development in Indole Derivatives as Anticancer Agent: A Mechanistic Approach. *Anticancer Agents Med. Chem.* **2021**, *21* (14), 1802−1824.
(67) Das, J.; Chen, P.; Norris, D.; Padmanabha, R.; Lin, J.; Moquin, R. V.; Shen, Z.; Cook, L. S.; Doweyko, A. M.; Pitt, S.; Pang, S.; Shen, D. R.; Fang, Q.; de Fex, H. F.; McIntyre, K. W.; Shuster, D. J.; Gillooly, K. M.; Behnia, K.; Schieven, G. L.; Wityak, J.; Barrish, J. C. 2-aminothiazole as a novel kinase inhibitor template. Structure-activity relationship studies toward the discovery of N-(2-chloro-6-methylphenyl)-2-[[6-[4-(2-hydroxyethyl)-1- piperazinyl)]-2-methyl-4-pyrimidinyl]amino)]-1,3-thiazole-5-carboxamide (dasatinib, BMS-354825) as a potent pan-Src kinase inhibitor. *J. Med. Chem.* **2006**, *49* (23), 6819−32.
(68) Das, J.; Padmanabha, R.; Ping, C., Cyclic protein tyrosine kinase inhibtors. CN 1348370A.
(69) McIntyre, J. A.; Castaner, J.; Bayes, M. Dasatinib. *Drugs Furture* **2006**, *31* (4), No. 0291.
(70) Yan, R., Yang, Hao, Hou, Wen, Xu, Yongxiang*Synthesis Process of Dasatinib and Intermediate. WO/2011/095126 A*2011.
(71) Menendez, C. A.; Mohamed, A.; Perez-Lemus, G. R.; Weiss, A. M.; Rawe, B. W.; Liu, G.; Crolais, A. E.; Kenna, E.; Byléhn, F.; Alvarado, W.; Mendels, D.; Rowan, S. J.; Tay, S.; de Pablo, J. J. Development of Masitinib Derivatives with Enhanced Mpro Ligand Efficiency and Reduced Cytotoxicity. *Molecules* **2023**, *28* (18), 6643.
(72) Brown, J. R., 3 Adriamycin and Related Anthracycline Antibiotics. In *Progress in Medicinal Chemistry*, Ellis, G. P.; West, G. B., Eds. Elsevier:1978; Vol. *15*, pp 125−164.
(73) *Daunorubicin*. https://go.drugbank.com/drugs/DB00694 (accessed 11th Dec 2023).
(74) *Zorubicin*. https://en.wikipedia.org/wiki/Zorubicin (accessed 11th Dec 2023).
(75) Fong, P. C.; Boss, D. S.; Yap, T. A.; Tutt, A.; Wu, P.; Mergui-Roelvink, M.; Mortimer, P.; Swaisland, H.; Lau, A.; O'Connor, M. J.; Ashworth, A.; Carmichael, J.; Kaye, S. B.; Schellens, J. H. M.; de Bono, J. S. Inhibition of Poly(ADP-Ribose) Polymerase in Tumors from BRCA Mutation Carriers. *New England Journal of Medicine* **2009**, *361* (2), 123−134.
(76) *Olaparib*. https://en.wikipedia.org/wiki/Olaparib (accessed 11th Dec 2023).
(77) Bailly, C. Toward a repositioning of the antibacterial drug nifuroxazide for cancer treatment. *Drug Discovery Today* **2019**, *24* (9), 1930−1936.
(78) *Nifuroxazide*. https://en.wikipedia.org/wiki/Nifuroxazide (accessed 11th Dec 2023).
(79) Timperio, A. M.; Kuiper, H. A.; Zolla, L. Identification of a furazolidone metabolite responsible for the inhibition of amino oxidases. *Xenobiotica* **2003**, *33* (2), 153−167.
(80) *Furazolidone*. https://en.wikipedia.org/wiki/Furazolidone (accessed 11th Dec 2023).
(81) Eldehna, W. M.; Al-Wabli, R. I.; Almutairi, M. S.; Keeton, A. B.; Piazza, G. A.; Abdel-Aziz, H. A.; Attia, M. I. Synthesis and biological evaluation of certain hydrazonoindolin-2-one derivatives as new potent anti-proliferative agents. *Journal of Enzyme Inhibition and Medicinal Chemistry* **2018**, *33* (1), 867−878.
(82) Ciufolini, M.; Wermuth, C.; Gielthen, B.; Moussy, A., 2-(3-aminoaryl) amino-4-aryl-thiazoles and their use as c-kit inhibitors. Google Patents: HK1084382A1 2005.
(83) Moussy, A.; Reginault, P.; Bellamy, F. O.; Lermet, A.Process for the synthesis of 2-aminothiazole compounds as kinase inhibitors. WO2008/98949, 2008.
(84) Moussy, A.; Kinet, J.-P.Use of c-kit inhibitors for treating type ii diabetes. WO2005/16323, 2005.
(85) Ciufolini, M.; Wermuth, C.; Gielthen, B.; Moussy, A.2-(3-Aminoaryl)amino-4-aryl-thiazoles and their use as c-kit inhibitors. WO2004/14903, 2004.
(86) Moussy, A.; Reginault, P.; Bellamy, F. o.; Lermet, A.Process for the synthesis of 2-aminothiazole compounds as kinase inhibitors. US2012/196871, 2012.
(87) Gaitonde, A.; Choudhari, B.; Bansode, P.; Phadtare, S.Novel process. WO2010/1167, 2010.
(88) Sun, L.; Liang, C.; Shirazian, S.; Zhou, Y.; Miller, T.; Cui, J.; Fukuda, J. Y.; Chu, J.-Y.; Nematalla, A.; Wang, X.; Chen, H.; Sistla, A.; Luu, T. C.; Tang, F.; Wei, J.; Tang, C. Discovery of 5-[5-fluoro-2-oxo-1,2-dihydroindol-(3Z)-ylidenemethyl]-2, 4-dimethyl-1H-pyrrole-3-carboxylic acid (2-diethylaminoethyl)amide, a novel tyrosine kinase inhibitor targeting vascular endothelial and platelet-derived growth factor receptor tyrosine kinase. *J. Med. Chem.* **2003**, *46* (7), 1116−1119.
(89) Zhu, J.A process for amidation of pyrrole carboxylate compounds. WO2011/110199, 2011.
(90) Dehury, S. K.; Dammalapati, V. L. N.; Indukuri, V. S. K.; Gorantla, S. R.An improved process for the preparation of sunitinib and its acid addition salts thereof. WO2013/140232, 2013.
(91) Dehury, S. K.; Dammalapati, V. L. N.; Indukuri, V. S. K.; Gorantla, S. R.Process for the perparation of sunitinib and its acid addition salts thereof. US2015/25252, 2015.
(92) Backos, D. S.; Casalvieri, K. A.; Jordan, C. T.; Matheson, C. J.; Minhajuddin, M.; Reigan, P. Substituted oxindol-3-ylidenes as AMP-activated protein kinase (AMPK) inhibitors. *Eur. J. Med. Chem.* **2020**, *197*, No. 112316.
(93) Wang, J.-Q.; Miller, K. D.; Sledge, G. W.; Zheng, Q.-H. Synthesis of [18F]SU11248, a new potential PET tracer for imaging cancer tyrosine kinase. *Bioorg. Med. Chem. Lett.* **2005**, *15* (19), 4380−4384.
(94) Manley, J. M.; Kalman, M. J.; Conway, B. G.; Ball, C. C.; Havens, J. L.; Vaidyanathan, R. Early amidation approach to 3-[(4-amido)pyrrol-2-yl]-2-indolinones. *J. Org. Chem.* **2003**, *68* (16), 6447−6450.

https://doi.org/10.1021/acsomega.4c06889
ACS Omega 2024, 9, 41944−41967

(95) Lombardo, L. J.; Lee, F. Y.; Chen, P.; Norris, D.; Barrish, J. C.; Behnia, K.; Castaneda, S.; Cornelius, L. A.; Das, J.; Doweyko, A. M.; Fairchild, C.; Hunt, J. T.; Inigo, I.; Johnston, K.; Kamath, A.; Kan, D.; Klei, H.; Marathe, P.; Pang, S.; Peterson, R.; Pitt, S.; Schieven, G. L.; Schmidt, R. J.; Tokarski, J.; Wen, M. L.; Wityak, J.; Borzilleri, R. M. Discovery of N-(2-chloro-6-methyl- phenyl)-2-(6-(4-(2-hydroxyeth-yl)- piperazin-1-yl)-2-methylpyrimidin-4- ylamino)thiazole-5-carbox-amide (BMS-354825), a dual Src/Abl kinase inhibitor with potent antitumor activity in preclinical assays. *J. Med. Chem.* **2004**, *47* (27), 6658−61.
(96) Co, B.-M. S., Process for preparing 2-aminothiazole-5-aromatic carboxamides as kinase inhibitors. JP 2007521340, WO 2005077945, US 2005215795, EP 1711481, US 2006004067, US 7491725.
(97) Co, B.-M.-S., Cyclic proein tyrosine kinase Inhibitors. JP 2002542193, WO 2000062778, US 6596746, EP 1610780, US 2004085388, US 2004054186, JP 2006523216, US 7125875.
(98) Co, B.-M.-S., Process for preparing 2-aminothiazole-5-carboxamides as kinase inhibitors. WO 2005176965.
(99) Peter, G. M. *Green's Protective groups in Organic Synthesis. 4edition,*John Wiley & Sons, Inc., *publication 16−3662*007.
(100) Li, J. C., Bang-chi; Smith, Daniel; Sun, Jung-hui,, Process for preparing N-(2-chloro-6-methylphenyl)-2-[[6-[4-(2-hydroxyethyl)-piperazin-1-yl[-2-methylpyrimidin-4-yl[amino[thiazole-5-carboxamide and related metabolites thereof. WO 2007/106879 A2.
(101) Amelia, T.; Kartasasmita, R. E.; Ohwada, T.; Tjahjono, D. H. Structural Insight and Development of EGFR Tyrosine Kinase Inhibitors. *Molecules* **2022**, *27* (3), 819.
(102) Callahan, R.; Hurvitz, S. Human epidermal growth factor receptor-2-positive breast cancer: Current management of early, advanced, and recurrent disease. *Curr. Opin Obstet Gynecol* **2011**, *23* (1), 37−43.
(103) Slamon, D. J.; Clark, G. M.; Wong, S. G.; Levin, W. J.; Ullrich, A.; McGuire, W. L. Human breast cancer: correlation of relapse and survival with amplification of the HER-2/neu oncogene. *Science* **1987**, *235* (4785), 177−82.
(104) Shibuya, M.; Claesson-Welsh, L. Signal transduction by VEGF receptors in regulation of angiogenesis and lymphangiogenesis. *Exp. Cell Res.* **2006**, *312* (5), 549−60.
(105) Dougher, M.; Terman, B. I. Autophosphorylation of KDR in the kinase domain is required for maximal VEGF-stimulated kinase activity and receptor internalization. *Oncogene* **1999**, *18* (8), 1619−27.
(106) Hubbard, S. R. Structural analysis of receptor tyrosine kinases. *Prog. Biophys. Mol. Biol.* **1999**, *71* (3−4), 343−58.
(107) Strawn, L. M.; Shawver, L. K. Tyrosine kinases in disease: overview of kinase inhibitors as therapeutic agents and current drugs in clinical trials. *Expert Opin Investig Drugs* **1998**, *7* (4), 553−73.
(108) Miyamoto, N.; Sakai, N.; Hirayama, T.; Miwa, K.; Oguro, Y.; Oki, H.; Okada, K.; Takagi, T.; Iwata, H.; Awazu, Y.; Yamasaki, S.; Takeuchi, T.; Miki, H.; Hori, A.; Imamura, S. Discovery of N-[5-({2-[(cyclopropylcarbonyl)amino]imidazo[1,2-b]pyridazin-6-yl}oxy)-2-methylphenyl]-1,3-dimethyl-1H-pyrazole-5-carboxamide (TAK-593), a highly potent VEGFR2 kinase inhibitor. *Bioorg. Med. Chem.* **2013**, *21* (8), 2333−2345.
(109) Zhang, J.; Gan, Y.; Li, H.; Yin, J.; He, X.; Lin, L.; Xu, S.; Fang, Z.; Kim, B. w.; Gao, L.; Ding, L.; Zhang, E.; Ma, X.; Li, J.; Li, L.; Xu, Y.; Horne, D.; Xu, R.; Yu, H.; Gu, Y.; Huang, W. Inhibition of the CDK2 and Cyclin A complex leads to autophagic degradation of CDK2 in cancer cells. *Nat. Commun.* **2022**, *13* (1), 2835.
(110) Cicenas, J.; Kalyan, K.; Sorokinas, A.; Stankunas, E.; Levy, J.; Meskinyte, I.; Stankevicius, V.; Kaupinis, A.; Valius, M. Roscovitine in cancer and other diseases. *Ann. Transl Med.* **2015**, *3* (10), 135.
(111) Schulze-Gahmen, U.; De Bondt, H. L.; Kim, S.-H. High-Resolution Crystal Structures of Human Cyclin-Dependent Kinase 2 with and without ATP: Bound Waters and Natural Ligand as Guides for Inhibitor Design. *J. Med. Chem.* **1996**, *39* (23), 4540−4546.
(112) Huang, S.-Y. Comprehensive assessment of flexible-ligand docking algorithms: current effectiveness and challenges. *Briefings in Bioinformatics* **2018**, *19* (5), 982−994.
(113) Ekins, S.; Waller, C. L.; Swaan, P. W.; Cruciani, G.; Wrighton, S. A.; Wikel, J. H. Progress in predicting human ADME parameters in silico. *J. Pharmacol Toxicol Methods* **2000**, *44* (1), 251−72.
(114) Lipinski, C. A.; Lombardo, F.; Dominy, B. W.; Feeney, P. J. Experimental and computational approaches to estimate solubility and permeability in drug discovery and development settings. *Adv. Drug Delivery Rev.* **1997**, *23* (1), 3−25.
(115) Ghose, A. K.; Viswanadhan, V. N.; Wendoloski, J. J. A knowledge-based approach in designing combinatorial or medicinal chemistry libraries for drug discovery. 1. A qualitative and quantitative characterization of known drug databases. *J. Comb Chem.* **1999**, *1* (1), 55−68.
(116) Jorgensen, W. L.; Duffy, E. M. Prediction of drug solubility from structure. *Adv. Drug Delivery Rev.* **2002**, *54* (3), 355−366.
(117) Chemi, G.; Gemma, S.; Campiani, G.; Brogi, S.; Butini, S.; Brindisi, M. Computational Tool for Fast in silico Evaluation of hERG K+ Channel Affinity. *Front. Chem.* **2017**, *5*, 7.
(118) Kulkarni, A.; Han, Y.; Hopfinger, A. J. Predicting Caco-2 Cell Permeation Coefficients of Organic Molecules Using Membrane-Interaction QSAR Analysis. *J. Chem. Inf. Comput. Sci.* **2002**, *42* (2), 331−342.
(119) Clark, D. E. In silico prediction of blood−brain barrier permeation. *Drug Discovery Today* **2003**, *8* (20), 927−933.
(120) Alotaibi, A. A.; Asiri, H. H.; Rahman, A. F. M. M.; Alanazi, M. M. Novel pyrrolo[2,3-d]pyrimidine derivatives as multi-kinase inhibitors with VEGFR-2 selectivity. *Journal of Saudi Chemical Society* **2023**, *27* (5), No. 101712.
(121) Alotaibi, A. A.; Alanazi, M. M.; Rahman, A. F. M. M. Discovery of New Pyrrolo[2,3-d]pyrimidine Derivatives as Potential Multi-Targeted Kinase Inhibitors and Apoptosis Inducers. *Pharmaceuticals* **2023**, *16* (9), 1324.
(122) DeLano, W. L.*The PyMOL molecular graphics system*; DeLano Scientific LLC: San Carlos, CA, USA, 2002.
(123) Trott, O.; Olson, A. J. AutoDock Vina: improving the speed and accuracy of docking with a new scoring function, efficient optimization, and multithreading. *J. Comput. Chem.* **2010**, *31* (2), 455−61.
(124) Butt, S. S.; Badshah, Y.; Shabbir, M.; Rafiq, M. Molecular Docking Using Chimera and Autodock Vina Software for Non-bioinformaticians. *JMIR Bioinformatics Biotechnol* **2020**, *1* (1), No. e14232.
(125) De Azevedo, W. F.; Leclerc, S.; Meijer, L.; Havlicek, L.; Strnad, M.; Kim, S.-H. Inhibition of Cyclin-Dependent Kinases by Purine Analogues. *Eur. J. Biochem.* **1997**, *243* (1−2), 518−526.

https://doi.org/10.1021/acsomega.4c06889
ACS Omega 2024, 9, 41944−41967